

# Wip1 inhibitor CCT007093 alleviates immune exhaustion of lymphocytes via p65 NF- $\kappa$ B and YY1 in chronic hepatitis B virus infection in mice

Yu-Syuan You<sup>1</sup>, Wan-Ting Chang<sup>1</sup>, Chia-Lang Hsu<sup>2</sup>, Yan-Fong Lu<sup>1</sup>, Hui-Ying Wang<sup>1</sup>, InKyeom Kim<sup>3</sup>, and Shiang-Jong Tzeng<sup>1</sup>

<sup>1</sup>National Taiwan University College of Medicine

<sup>2</sup>National Taiwan University Hospital

<sup>3</sup>Kyungpook National University School of Medicine

April 08, 2024

## Abstract

**Background and Purpose:** Prolonged viral infections often lead to lymphocyte exhaustion, marked by heightened inhibitory receptor expression like PD-1, compromising host defense mechanisms. Although monoclonal antibodies like anti-PD-1 can alleviate exhausted lymphocytes, their cost limits widespread use. The unexplored potential of chemical checkpoint inhibitors in rejuvenating immune responses prompted our investigation. **Experimental Approach:** We focused on CCT007093, a Wip1 inhibitor, screened out for its unique ability to concurrently reduce PD-1 and Fc $\gamma$ RIIB expression, using a murine model of immune exhaustion induced by chronic hepatitis B virus (HBV) infection. **Key Results:** CCT007093 treatment to HBV-infected mice resulted in decreased levels of PD-1 expression, resulting in reduced percentages of PD-1+/hi CD4 and CD8 T cells in circulation, spleen, and liver. PD-1 and Fc $\gamma$ RIIB expression, alongside the percentages of PD-1+/hi and Fc $\gamma$ RIIB+/hi CD19+ B cells in these tissues, were similarly diminished. Moreover, CCT007093-treated intrahepatic lymphocytes exhibited heightened responsiveness to ex vivo activation. Together, serum HBsAg levels were significantly reduced in treated mice compared to controls. Detailed analysis uncovered p65 NF- $\kappa$ B as the primary activator of T cells and B cells, while YY1 emerged as the key regulator, orchestrating the down-regulation of PD-1 and Fc $\gamma$ RIIB gene transcription in response to CCT007093. **Conclusions and Implications:** Our study highlights CCT007093's pharmacological efficacy in mitigating immune exhaustion in HBV-infected mice, selectively enhancing adaptive immunity. Beyond antiviral applications, it underscores the prowess of chemical checkpoint inhibitors, exemplified by CCT007093, in alleviating immune exhaustion induced by viruses and potentially in various cancers.

**Wip1 inhibitor CCT007093 alleviates immune exhaustion of lymphocytes via p65 NF- $\kappa$ B and YY1 in chronic hepatitis B virus infection in mice**

**Authors:**

Yu-Syuan You<sup>1</sup>, Wan-Ting Chang<sup>1</sup>, Chia-Lang Hsu<sup>1</sup>, Yan-Fong Lu<sup>1,3</sup>, Hui-Ying Wang<sup>1</sup>, InKyeom Kim<sup>4,5,6</sup>, Shiang-Jong Tzeng<sup>1</sup>

**Affiliations:**

<sup>1</sup>Graduate Institute of Pharmacology, College of Medicine, National Taiwan University, Taipei, Taiwan

<sup>2</sup>Department of Medical Research, National Taiwan University Hospital, Taipei, Taiwan

<sup>3</sup>Department of Obstetrics and Gynecology, Shin-Kong Wu Ho-Su Memorial Hospital, Taipei, Taiwan

<sup>4</sup>Department of Pharmacology, <sup>5</sup>BK21 Plus KNU Biomedical Convergence Program,

<sup>6</sup>Cardiovascular Research Institute, School of Medicine, Kyungpook National University, 41944, Republic of Korea

**Running Title**

CCT007093 alleviates HBV-induced immune exhaustion

**Corresponding author**

<sup>1</sup>Correspondence to Shiang-Jong Tzeng

Address: Room 1118, No.1, Section 1, Ren-Ai Road, Taipei 10051, Taiwan

Email: [sjtzeng@ntu.edu.tw](mailto:sjtzeng@ntu.edu.tw)

Phone: 1-886-2-23123456 ext. 288314

Fax: 1-886-2-24915297

## **Abstract**

**Background and Purpose:** Prolonged viral infections often lead to lymphocyte exhaustion, marked by heightened inhibitory receptor expression like PD-1, compromising host defense mechanisms. Although monoclonal antibodies like anti-PD-1 can alleviate exhausted lymphocytes, their cost limits widespread use. The unexplored potential of chemical checkpoint inhibitors in rejuvenating immune responses prompted our investigation.

**Experimental Approach:** We focused on CCT007093, a Wip1 inhibitor, screened out for its unique ability to concurrently reduce PD-1 and FcγRIIB expression, using a murine model of immune exhaustion induced by chronic hepatitis B virus (HBV) infection.

**Key Results:** CCT007093 treatment to HBV-infected mice resulted in decreased levels of PD-1 expression, resulting in reduced percentages of PD-1<sup>+/hi</sup> CD4 and CD8 T cells in circulation, spleen, and liver. PD-1 and FcγRIIB expression, alongside the percentages of PD-1<sup>+/hi</sup> and FcγRIIB<sup>+/hi</sup> CD19<sup>+</sup> B cells in these tissues, were similarly diminished. Moreover, CCT007093-treated intrahepatic lymphocytes exhibited heightened responsiveness to *ex vivo* activation. Together, serum HBsAg levels were significantly reduced in treated mice compared to controls. Detailed analysis uncovered p65 NF-κB as the primary activator of T cells and B cells, while YY1 emerged as the key regulator, orchestrating the down-regulation of PD-1 and FcγRIIB gene transcription in response to CCT007093.

**Conclusions and Implications:**

Our study highlights CCT007093's pharmacological efficacy in mitigating immune exhaustion in HBV-infected mice, selectively enhancing adaptive immunity. Beyond antiviral applications, it underscores the prowess of chemical checkpoint inhibitors, exemplified by CCT007093, in alleviating immune exhaustion induced by viruses and potentially in various cancers.

**Keywords**

CCT007093, Checkpoint inhibitors, Fc $\gamma$ RIIB, Hepatitis B virus (HBV), Immune exhaustion, PD-1, Ying Yang 1 (YY1)

**Bullet point summary:****What is already known**

- Blocking antibodies of checkpoint molecules alleviates immune exhaustion in patients with viral infection and cancers.
- Current monoclonal antibodies like anti-PD-1 for checkpoint blockade is expensive, limiting their widespread use.

**What this study adds**

- CCT007093 downregulates expression of PD-1 and FcγRIIB in lymphocytes to ameliorate immune exhaustion.
- CCT007093 regulates transcription of PD-1 and FcγRIIB genes via enhancing p65 NF-κB and blocking YY1.

**Clinical significance**

- Chemical checkpoint inhibitors show promise in addressing immune exhaustion of lymphocytes in chronic HBV-infected mice.
- Chemical checkpoint inhibitors can alleviate immune exhaustion induced by viruses and potentially in various cancers.

## **Introduction**

During chronic viral infections, the immune response can be hindered by immune exhaustion, characterized by the increased expression of inhibitory receptors on lymphocytes, such as cytotoxic T-lymphocyte-associated protein 4 (CTLA4), programmed death-1 (PD-1), and programmed death-ligand 1 (PD-L1). This exhaustion negatively affects the activation, proliferation, and differentiation of lymphocytes (1, 2). In chronic HBV infection, both CD4 and CD8 T cells show elevated levels of PD-1, indicating T cell exhaustion (3, 4). Similarly, B cells in HIV-infected patients exhibit exhaustion with increased expression of FcγRIIB, leading to impaired B cell function and antibody (Ab) production (5). Taken together, T-cell exhaustion weakens the cytotoxic response necessary for clearing the virus, while B-cell exhaustion compromises the effectiveness of the humoral response against the virus. However, the factors that can ameliorate or reverse lymphocyte exhaustion in order to promote activation of T cells and B cells in chronic viral infections for the treatment of patients require further research.

Recovering from immune exhaustion in persistent viral infections represents a primary objective in the advancement of novel therapeutics. Research has generated compelling evidence endorsing the targeting of inhibitory receptors with checkpoint inhibitors, such as the use of monoclonal Abs aimed at PD-1, which has proven effective in enhancing T cell functionality in individuals with human HIV and HBV infections (6, 7). Additionally, the remarkable success of anti-PD-1 and anti-PD-L1 monoclonal Abs in cancer therapy underscores the potential importance of targeting these pathways for the prevention and management of various infectious diseases (8-10). While antiviral drugs continue to be the mainstay treatment for immune exhaustion and chronic viral infections,

immune checkpoint inhibitors like anti-PD-1 have emerged as potential therapeutic options. However, the effectiveness of antiviral drugs in combating immune exhaustion remains uncertain. Additionally, the widespread use of checkpoint inhibitors is hindered by factors such as high cost, long circulating half-life, and the potential for severe side effects, including life-threatening cytokine storms. Therefore, further research and development of safer and more cost-effective therapies are necessary to address immune exhaustion and chronic viral infections effectively.

Chemical compounds offer an alternative approach to deliver immune checkpoint inhibition, addressing some of the challenges associated with monoclonal Ab inhibitors. Chemical compounds generally have a faster turnover rate than monoclonal Abs in circulation, making them potentially more suitable for therapeutic applications. Furthermore, the risk of cytokine storms may be reduced compared to monoclonal Ab-based therapies. Importantly, they can be manufactured more easily and at a lower cost, allowing for broader accessibility for patients. Therefore, the development of chemical compounds as immune checkpoint inhibitors holds promise for overcoming the limitations of monoclonal Abs and improving the treatment of immune exhaustion and chronic viral infections.

By employing a cell-based gene promoter reporter assay, we conducted a screen of compounds with the capability to reduce the gene transcription of both FcγRIIB and PD-1 in BJAB B cells (11). From the pool of candidate compounds identified, our focus narrowed to CCT007093, an inhibitor of wild-type p53-induced phosphatase 1 (Wip1, also known as PPM1D). Wip1 is a serine/threonine phosphatase mainly localized in the nucleus (12). To assess the potential of CCT007093 in countering immune exhaustion within the



context of chronic viral infection, we harnessed an established murine model of chronic hepatitis B virus (HBV) infection for therapeutic and mechanistic investigations (13).

## **Methods**

### **Reagents**

CCT007093 (IC<sub>50</sub>: 8.4  $\mu$ M) and DMSO were purchased from Selleckchem (Houston, TX, USA). Recombinant HBsAg and HBcAg proteins were acquired from Sino Biological. For immunoblotting, specific Abs to detect p65 NF- $\kappa$ B, phospho-p65 NF- $\kappa$ B (Ser 536), p53, phospho-p53 (Ser 15), and Wip1 were purchased from Cell Signaling Technology (Beverly, MA, USA). Anti-PD-1 and anti-YY1 Abs were purchased from Santa Cruz (Santa Cruz, CA, USA), while anti-Fc $\gamma$ RIIB Ab was ordered from Genetex Inc. (Irvin, CA, USA). Cell activation kit (ionomycin + PMA (phorbol-12-myristate-13-acetate)) and anti-IFN- $\gamma$  Abs were purchased from Biolegend. Anti- $\beta$ -actin Ab was ordered from Novus Biologicals (Littleton, CO, USA). Anti-myc Ab was purchased from Proteintech (Rosemont, IL, USA). The protein G-sepharose beads were sourced from Sigma-Aldrich (St. Louis, MO, USA). Both horseradish peroxidase-conjugated goat anti-rabbit and anti-mouse Abs were obtained from Jackson ImmunoResearch (West Grove, PA, USA). Monoclonal Abs for flow cytometry were ordered from Biolegend and BD Biosciences (Becton, NJ, USA).

### **Plasmids**

The HBc175 mutant pAAV/HBV1.2 construct was generously provided by Dr. Pei-Jer Chen at National Taiwan University. This construct expresses HBcAg proteins with a

C-terminal deletion of 10 amino acids (13). The Wip1 cDNA plasmid (GV227-Wip1) was obtained from GeneChem (Shanghai, China) and subsequently subcloned into the pcDNA3.1/myc-His B vector. The pCMV6-XL5-YY1 plasmid was acquired from Origene (Rockville, MD, USA). Serum HBsAg levels were measured with an AXSYM system kit (Abbott GmbH Diagnostica, Wiesbaden, Germany).

### **Animals and hydrodynamic injection**

Male C57BL/6J mice, aged 5 to 6 weeks, were acquired from the Center for Laboratory Animals of the College of Medicine, National Taiwan University (NTU). These mice were housed under specific pathogen-free conditions. All animal experiments were conducted in accordance with ethical guidelines and approved protocols from the Institutional Animal Care and Use Committee (IACUC) of the College of Medicine, NTU, under the protocol numbers: 20130228 and 20170401. The hydrodynamic injection procedure, aimed at inducing HBV-associated immune exhaustion in mice, has been previously documented (13). In brief, we administered 10 µg of purified HBc175 plasmid DNAs in approximately 1.5 ml PBS (equivalent to 8% of each mouse's body weight) via the tail vein, resulting in rapid hepatocyte rupture for *in vivo* transfection. Commencing four weeks after the hydrodynamic injection, serum levels of HBsAg in mice were monitored at 2-week intervals using an AXSYM system kit (Abbott GmbH Diagnostica, Wiesbaden, Germany). The persistence of HBsAg in the serum four weeks post-injection indicates the successful induction of chronic HBV infection and immune exhaustion. This method allows for the persistence of HBV for over one year in a considerable number of mice (8, 13).

### **Cell preparation from blood, spleen and liver**

Mouse blood was collected by puncturing the submandibular vein using lancets, with the blood being collected into a K<sub>2</sub>EDTA-coated tube (BD Biosciences). Splenocytes were isolated as previously detailed (14-17). To isolate intrahepatic leukocytes, the mouse liver was minced using scissors. Sections of the liver were placed into two 10-cm petri dishes, each containing 10 ml of digestion buffer (0.04% collagenase IV and 0.002% DNase I dissolved in PBS). The liver pieces were gently crushed with a sterile syringe plunger and passed through a 100- $\mu$ m cell strainer to eliminate connective tissues. The liver suspensions were then incubated at 37°C for 45 min in an incubator. Subsequent to incubation, the liver cell mixture was collected into a 50 ml conical tube and centrifuged at 30 $\times$ g (500 rpm) for 3 min to separate hepatocytes. Following centrifugation, the cell pellets were re-suspended in RBC lysis buffer and incubated at room temperature for 5 min to eliminate erythrocytes. This was followed by another centrifugation at 2,200 rpm for 15 min. The pellets were then re-suspended in 4 ml of PBS and cautiously layered onto the top of a Percoll gradient, containing 4 ml of 25% Percoll solution (GE Healthcare, Piscataway, NJ). The layer of 25% Percoll was placed over the 4 ml of 80% Percoll in a 15 ml tube. The cells were then centrifuged at 2,500 rpm at 25°C for 25 min. The intrahepatic leukocytes were carefully collected from the interface between the 25% and 80% Percoll layers and subsequently washed with 10 ml of PBS. Following a centrifugation step at 2,200 rpm for 10 min, the resulting cell pellets were harvested for subsequent flow cytometric analysis.

### **Flow cytometry**

For T cells, specific Abs of CD3-APC-Cy7 (clone 145-2C11), CD4-Alexa 647 (clone GK1.5), CD8-BV510 (clone 53-6.7), PD-1-PE (clone 29F.1A12) and CD127-FITC (clone A7R34) were added and incubated at 4°C for 20 min. For B cells, the CD16/32-FITC Abs (clone 2.4G2) were initially added for a 5-min incubation period, followed by an additional 20-min incubation with CD19-PE-Cy7 (clone 6D5) and PD-1-PE Abs at 4°C. For intracellular staining, isolated intrahepatic leukocytes ( $5 \times 10^6/\text{ml}$ ) were cultured in the presence of a stimulation agent cocktail for a duration of 3 hr. Subsequently, the cells were collected and labeled with CD3-APC-Cy7 (clone 145-2C11), CD4-PerCP-Cy5.5 (clone RM 4-5), and CD8-BB515 (clone 53-6.7) Abs on ice for a period of 20 min. Following the completion of the staining process, the cells were subjected to permeabilization and fixation using a fixation/permeabilization solution (BD Biosciences) for 20 min on ice. This was followed by the addition of IFN- $\gamma$ -PE (clone XMG1.2) or rat IgG1-PE isotype (clone G0114F7) Abs, with an additional 30-min incubation on ice. After the necessary washing steps, the cells were analyzed using flow cytometry.

### **Enzyme-linked immunospot (ELISPOT)**

ELISPOT plates (BD Biosciences) were coated overnight at 4°C with recombinant HBsAg or HBcAg proteins (Sino Biological) at a concentration of 2  $\mu\text{g}/\text{ml}$ . Approximately  $10^5$  purified intrahepatic leukocytes was used for the ELISPOT assay, and the experiments were conducted following previously described protocols (16).

### **Cell culture and dual-luciferase reporter assay**

BJAB B cells is a Epstein-Barr virus-negative Burkitt-like lymphoma cell line<sup>17</sup>. Jurkat T cells and HEK293T cells were grown in RPMI 1640 medium supplemented with 10% fetal bovine serum and penicillin/streptomycin/Amphotericin B, and maintained in an incubator with 5% of CO<sub>2</sub> at 37°C. The dual-luciferase reporter system from Promega (Madison, WI, USA) was utilized to measure the transcriptional activities of promoters. For cell transfection, the Amaxa<sup>TM</sup> Nucleofector kit V from Lonza (Basel, Switzerland) was used. Briefly, 1×10<sup>7</sup> BJAB B cells were transfected with 20 µg of pGL3 luciferase reporter plasmids containing 2,200 bp, 1,636 bp, 1,075 bp and 926 bp promoter sequences upstream of ATG of PD-1 gene (Genebank access no. AF363458), respectively. Simultaneously, the *renilla* luciferase reporter constructs (500 ng) was co-transfected as internal controls for transfection efficiency and for normalization of luciferase activities. Following cell electroporation for 4 hr, cells were treated with vehicle, 2 or 5 µM CCT007093 in triplicates and incubated for an additional 24 hr. Cells were lysed, and luciferase activities were measured using the dual-luciferase reporter kit (Promega) following the manufacturer's instructions. Luciferase activities were presented as the ratio of firefly to *renilla* luciferase activities (Fluc/Rluc). Similarly, the 1.5 kb and 0.6 kb promoter sequences of FcγRIIB gene (Genebank access no. AF433951) were linked to firefly luciferase constructs for similar analysis.

### **Western blotting and immunoprecipitation**

The western blotting procedures followed standard methods. BJAB B cells were lysed in RIPA buffer containing protease and phosphatase inhibitor cocktails on ice for 30 min, followed by a brief sonication. Cell lysates were then centrifuged at 12,000×g at 4°C for

15 min, and the resulting supernatant was transferred into a new Eppendorf tube. Protein concentration was determined using the Coomassie blue assay kit (Thermo Fisher) according to the manufacturer's instructions. Proteins in lysates were separated by SDS-polyacrylamide gel electrophoresis (PAGE; 8%-10%). After the gel transfer, membranes were blocked with TBS-T buffer (50 mM Tris-HCl, pH 7.6, 150 mM NaCl and 0.1% Tween 20) containing 5% non-fat milk at ambient temperature for 1 hr to reduce non-specific protein binding. Primary Abs were added and incubated overnight at 4°C. Following three washes with TBS-T, HRP-conjugated secondary Abs (Jackson ImmunoResearch) were added and incubated at ambient temperature for 1 hr. After completing incubation, membranes were washed six times with TBS-T. Protein bands specific to the Abs were detected using a chemiluminescence ECL kit. The  $\beta$ -actin was used as an internal control.

HEK 293T cells ( $2.4 \times 10^5$ /ml) were seeded in 6-well plates and allowed to grow for 24 hr prior to transfection. For transfection, the culture medium in each well was replaced with a mixture of full and serum-free media at a ratio of 1:1 (200  $\mu$ l), along with 4  $\mu$ g of each plasmid in 8  $\mu$ l of TurboFect transfection reagent (Thermo Fisher Scientific). After incubation at 37°C for 24 hr, the cells were harvested for western blotting analysis as described earlier. For immunoprecipitation, protein G-sepharose beads (20  $\mu$ l) were added to each sample (500  $\mu$ g) and incubated overnight at 4°C. The Ab-specific immune complexes were then washed with cold lysis buffer and TBS-T containing protease and phosphatase inhibitors. After boiling in the sample loading buffer for 10 min, the samples were resolved in 8%-10% SDS-PAGE gels for subsequent western blotting.

### **RNA extraction and sequencing of splenic B cells**

Total RNAs of Jurkat T cells and BJAB B cells were extracted for RNA-sequencing following the established protocol (15, 18). RNA was extracted using Trizol. The purified RNA was utilized for library preparation using the TruSeq stranded mRNA library prep kit (Illumina, San Diego, CA, USA), following the manufacturer's instructions. Briefly, mRNA was purified from 1 µg of total RNA using oligo(dT)-coupled magnetic beads and fragmented into smaller fragments. The first-strand cDNA was synthesized using reverse transcriptase and random primers. Double-stranded cDNA was generated, and the DNA fragments' 3' ends were adenylation-modified. Adaptors were ligated to the fragments, which were subsequently purified using the AMPure XP system (Beckman Coulter, Beverly, USA). The quality of the libraries was assessed using the Agilent Bioanalyzer 2100 system and real-time PCR. qualified libraries were sequenced on an Illumina NovaSeq 6000 platform, generating 150 bp paired-end reads, by Genomics, BioSci & Tech Co., New Taipei City, Taiwan.

### **Bioinformatic analysis**

The raw reads underwent quality checking using FastQC (v0.11.9), and adaptor sequences as well as low-quality reads were eliminated using cutadapt (v3.5). The qualified reads were then aligned to the mouse reference genome GRCh38 using STAR (v2.7.8a) with the two-pass mode (19). Gene-level read counts were calculated based on the Gencode v35 annotation. Cross-sample normalization was conducted using the TMM (Trimmed Mean of the M-values) method implemented in the R package edgeR (20), and transcript per million (TPM) values were calculated for further analysis. Differential expression analysis was performed using the R package NOISeq (21), and genes with a probability

greater than or equal to 0.4 were considered as differentially expressed genes. Pre-rank gene-set enrichment analysis (GSEA) was carried out using the functions of the R package clusterProfiler (22) on gene-sets sourced from MSigDB (v7.4) (23). Genes were ranked based on the rank \* probability, where the rank and probability values were obtained from the NOISeq results. Pathway enrichment and functional associated networks were constructed using the Ingenuity Pathway Analysis (IPA).

### **Statistical analysis**

FlowJo software and Student's *t*-test was used to analyze flow cytometric data. Plots were generated using GraphPad Prism 7.0 (GraphPad Software Inc., USA) and the results were presented as mean  $\pm$  standard error (SEM). P-values below 0.05 are considered statistically significant between compared groups and denoted by asterisks: \**p* < 0.05, \*\**p* < 0.01, and \*\*\**p* < 0.001.

### **Results**

#### **CCT007093 treatment reduced serum HBsAg levels in chronic HBV-infected mice**

In our research, we employed a well-established murine model of chronic HBV infection characterized by T-cell exhaustion to evaluate the therapeutic potential of CCT007093. We chose male C57BL/6 mice because they exhibit a significantly higher prevalence of HBV infection, mirroring the clinical scenario (13, 24). The mice were treated with either a vehicle or CCT007093, administered at a dose of 3.5 mg/kg, via hydrodynamic injection of HBc175 plasmids. The treatment protocol, which extended over



14 days, commenced 8 weeks after the initiation of immune exhaustion (Fig. 1A). T-cell exhaustion was confirmed in this model by the increased expression of PD-1 in T cells and the sustained presence of serum HBsAg as previously described<sup>8</sup>. At the conclusion of the study, the mice were sacrificed to assess the restoration of immune function, as indicated by cell phenotypes and functions. As shown in Fig. 1B, mice infected with HBV and treated with CCT007093 exhibited a notable decrease in serum HBsAg levels compared to those that received the vehicle treatment alone. This reduction highlights the substantial therapeutic benefits linked to CCT007093 treatment.

### **CCT007093 downregulated PD-1 and FcγRIIB expression in lymphocytes in blood, spleen and liver of chronic HBV-infected mice**

We then conducted a flow cytometry analysis to assess the surface expression levels of PD-1 and FcγRIIB on both CD4 and CD8 T cells, as well as B cells, in the peripheral blood, spleen, and liver using flow cytometry. Our results revealed a significant reduction in the surface expression of PD-1 on circulating CD4 ( Fig. 2A) and CD8 (Fig. 2B) T cells, accompanied by a decrease in the respective percentages of PD-1<sup>+hi</sup> CD4 and CD8 T cells in mice treated with CCT007093. Additionally, B cells showed decreased surface expression levels of both PD-1 (Fig. 2C) and FcγRIIB (Fig. 2D) in the peripheral blood. Consequently, the respective percentages of PD-1<sup>+hi</sup> and FcγRIIB<sup>+hi</sup> CD19<sup>+</sup> B cells also significantly decreased in mice treated with CCT007093 (Fig. 2C, 2D).

When analyzing splenic leukocytes, we observed that the expression levels of PD-1 on CD4 and CD8 (Fig. 3A) T cells, as quantified by MFI, as well as the respective percentages of PD-1<sup>+hi</sup> CD4 and CD8 T cells, were significantly reduced in mice treated

with CCT007093 (Fig. 3A). Notably, recent studies have indicated that HBV-specific dysfunctional T cells exhibit high PD-1 levels coupled with low CD127 (also known as IL-7 receptor) expression in both chronic HBV patients and mice (8, 25). To delve deeper into this, we compared the frequency of exhausted splenic T cells, defined as PD-1<sup>+hi</sup>CD127<sup>lo</sup>CD4<sup>+</sup> and PD-1<sup>+hi</sup>CD127<sup>lo</sup>CD8<sup>+</sup> T cells, between the vehicle and CCT007093-treated mice. Following CCT007093 treatment, the percentages of these exhausted T cell populations were significantly reduced in comparison to those in the vehicle-treated mice (Fig. 3B). Additionally, CCT007093 treatment led to markedly lower expression levels and percentages of PD-1<sup>+hi</sup> B cells and FcγRIIB<sup>+hi</sup> B cells in the spleen compared to the vehicle-treated mice (Fig. 3C).

To assess the localized therapeutic effects of CCT007093 within the liver, we conducted an analysis of intrahepatic leukocytes obtained from HBV-infected mice. As depicted in Fig. 4, the expression levels and percentages of PD-1<sup>+hi</sup> CD4 T cells and CD8 T cells were markedly reduced in CCT007093-treated mice in comparison to vehicle-treated mice. In alignment with our findings in the spleen (Fig. 3), the percentages of intrahepatic PD-1<sup>+hi</sup>CD127<sup>lo</sup>CD4<sup>+</sup> and PD-1<sup>+hi</sup>CD127<sup>lo</sup>CD8<sup>+</sup> T cells were significantly lower in CCT007093-treated mice than in vehicle-treated mice (Fig. 4A, 4B). Moreover, the expression levels and percentages of PD-1<sup>+hi</sup> B cells and FcγRIIB<sup>+hi</sup> B cells were also substantially lower in CCT007093-treated mice than in vehicle-treated mice (Fig. 4C).

### **CCT007093 treatment enhanced IFN-γ and antiviral Ab production by intrahepatic lymphocytes in HBV-infected mice**

Given that the increased expression of inhibitory receptors can lead to compromised functionality, including diminished IFN- $\gamma$  production and reduced plasma cell (PC) numbers (26-28), we sought to investigate whether the downregulation of PD-1 and Fc $\gamma$ RIIB expression in intrahepatic lymphocytes following CCT007093 treatment could enhance IFN- $\gamma$  production in T cells and boost the synthesis of antiviral Abs by B cells. This could potentially revitalize the immune response and alleviate immune exhaustion. To explore this, we cultured purified intrahepatic leukocytes sourced from chronic HBV-infected mice and stimulated them with PMA and ionomycin for 3 hr. Following stimulation, we performed permeabilization and staining T cells using anti-IFN- $\gamma$  Abs. As a result, we observed an increased frequency of IFN- $\gamma^{+hi}$ CD4<sup>+</sup> T cells (Fig. 5A) and IFN- $\gamma^{+hi}$ CD8<sup>+</sup> T cells (Fig. 5B) in the CCT007093-treated group. These findings shed light on the potential of CCT007093 to enhance the cytotoxicity of T cells in the liver, potentially ameliorating immune exhaustion in chronic HBV-infected mice.

The role of T cells in eliminating the HBV virus is of paramount importance, but the contribution of B cells should not be underestimated. B cells are instrumental in the defense against viral infections by generating neutralizing Abs, thereby providing an Ab-dependent shield against the infection (29, 30). Our investigation extends beyond T cells to encompass B cells, aiming to determine whether the reduced expression of Fc $\gamma$ RIIB within intrahepatic B cells, as a result of CCT007093 treatment, could influence PC production. To assess Ab-secreting cells (ASCs), we carried out ELISPOT assays. As shown in Fig. 5C, mice treated with CCT007093 exhibited a significant increase in the numbers of HBsAg- and HBcAg-specific ASCs. This finding suggests that CCT007093 mediates an enhancement in the humoral protective response within the liver.

### **Down-regulation of transcriptional activities of PD-1 and FcγRIIB genes by CCT007093 treatment**

To delve deeper into the inhibitory effects of CCT007093 on Wip1 and its potential substrates, such as p53 and NF-κB, recognized as transcription factors (12), we performed a comprehensive promoter analysis to investigate the transcriptional regulation of PD-1 and FcγRIIB genes. Analysis of the 2.2 kb promoter region upstream of transcriptional start site of the PD-1 gene identified potential transcriptional regulators, including p53, GATA, cAMP response element-binding protein (CREB), activator protein 1 (AP-1), Yin Yang 1 (YY1) and NF-κB (Fig. 6A). Similarly, the analysis of the 1.5 kb promoter region upstream of the transcriptional start site of the FcγRIIB gene revealed transcriptional regulators such as p53, AP-1, YY1 and NF-κB (Fig. 6B).

Using this information, we conducted luciferase reporter gene assays to assess the transcriptional activity of these promoters. We generated various 5' deletion mutants of the PD-1 and FcγRIIB gene promoters and inserted them into a firefly luciferase reporter construct for subsequent transfection experiments. The transcriptional activities of the PD-1 gene's -2,200 bp, -1,636 bp, -1,075 bp, and -936 bp promoter constructs, as well as the FcγRIIB gene's -1,522 bp, and -600 bp promoter constructs in BJAB B cells, both in the absence or presence of 2 or 5 μM of CCT007093 for 24 hr. The combined results indicated that the shortest promoters, specifically the -936 bp of the PD-1 gene and the -600 bp of FcγRIIB gene, retained their susceptibility to CCT007093 inhibition (Fig. 6C). Comparative analysis of these two promoter regions highlighted the co-existence of YY1

and NF- $\kappa$ B, suggesting their potential roles as critical co-transcriptional regulators in the context of CCT007093 response.

### **Effects of CCT007093 on the phosphorylation of transcriptional regulator substrates of Wip1**

Given the concurrent down-regulation of PD-1 and Fc $\gamma$ RIIB expression in T cells and B cells following CCT007093 treatment *in vivo* (Fig. 2-4), it seems plausible to hypothesize the existence of co-regulators governing the transcription of these two genes. Our promoter analysis of the PD-1 and Fc $\gamma$ RIIB genes suggests primary candidates for such transcriptional co-regulators are YY1 and NF- $\kappa$ B (Fig. 6).

Subsequently, we embarked on investigations to probe the effects of CCT007093 treatment on BJAB B cells through western blotting. According to literature findings, Wip1 targets the catalytic sites of p65 NF- $\kappa$ B and p53 at serine 535 and serine 15, respectively (12). To investigate this, BJAB B cells underwent treatment with varying CCT007093 concentrations (0, 5, 10 or 25  $\mu$ M) for durations of 15 min, 1 hr and 6 hr for western blot analysis. As shown in Fig. 7A, PD-1 and Fc $\gamma$ RIIB protein levels notably decreased at 6 hr in a dose-dependent manner. Wip1 inhibition by CCT007093 led to an initial increase in p-p65 NF- $\kappa$ B (S535) phosphorylation at 15 min, although this effect was transient, reverting to basal phosphorylation levels by the 6-hour mark. On the contrary, p53 (Ser 15) phosphorylation was observed at 1 hr and persisted up to 6 hr. It is important to note that, despite the inhibition of Wip1's phosphatase activity, the expression levels of Wip1 were unaffected by CCT007093 (Fig. 7A).

Moreover, our study also suggests YY1 might be a novel substrate of Wip1. We subsequently investigated if YY1 could directly interact with Wip1 within cells. As illustrated in Fig. 7B, our co-transfection experiments in HEK293T cells showed a clear interaction between YY1 and Wip1, confirmed through co-immunoprecipitation. This finding implies that CCT007093 treatment may boost the phosphorylation of serine and/or threonine residues of YY1 by inhibiting Wip1.

### **CCT007093-induced transcriptional regulatory pathways revealed by RNA-sequencing in T and B cells**

Given the identification of multiple substrates for Wip1 and the intricate network of transcription factors implicated in the regulation of PD-1 and Fc $\gamma$ RIIB expression, as suggested by the promoter analysis and reporter gene assays (Fig. 7), we performed bulk RNA-sequencing on Jurkat T cells and BJAB B cells. These cells were treated with either vehicle or 25  $\mu$ M of CCT007093 for 16 hr. Whole transcriptomic sequencing and subsequent analyses revealed a set of shared up-regulated and down-regulated genes in both cell types (Fig. 8A, 8B and Suppl. Table 1). Functional characterization of these genes through Gene Set Enrichment Analysis (GSEA) and Ingenuity Pathway Analysis (IPA) indicated their involvement in sterol metabolism pathways, such as the sterol regulatory binding protein (SREBP) pathway known to activate T cells and B cells (31, 32), and cytokine-driven pro-inflammatory pathways activated by CCT007093 stimulation (Fig. 8C). Notably, these up-regulated pathways are closely associated with activation of p65 NF- $\kappa$ B (33), which had been earlier identified as a potential key transcription co-regulator in the promoter analysis of PD-1 and Fc $\gamma$ RIIB genes (Fig. 8D). Conversely, another key

co-regulator, YY1, exhibited a positive correlation with the transcription factor-regulated pathway in Jurkat T cells (Fig. 8D). Additional investigation through GSEA unveiled further potential transcriptional regulators, including TP53 and AP-1, which exhibited significant binding sites on the PD-1 and FcγRIIB promoters (Fig. 6), activating their target genes in either Jurkat T cells, BJAB B cells, or both (Suppl. Fig. 1 and Suppl. Table 2).

## Conclusions and Discussion

Previous studies have demonstrated that PD-1/PD-L1 checkpoint blockades with blocking monoclonal Abs can restore antiviral intrahepatic T-cell responses in humans and in mice (7,8). It is then reasonable to hypothesize that chemical compounds capable of down-regulating the expression of these inhibitory receptors, such as PD-1 and FcγRIIB, could yield beneficial effects on the activation of T cells and B cells. In this study we present compelling evidence for the therapeutic potential of CCT007093 in mitigating immune exhaustion of lymphocytes induced by HBV infection in mice. Our results strongly support the capacity of CCT007093 to effectively reduce the elevated expression levels of both PD-1 and FcγRIIB, a phenomenon observed not only in the peripheral blood and spleen but significantly in the liver as well (Fig. 1-4). Furthermore, *ex vivo* analysis reveals enhanced activation of T cells with increased IFN-γ production and heightened antiviral Ab secretion by B cells (Fig. 5).

The mechanisms underlying CCT007093's ability to inhibit Wip1, subsequently down-regulating PD-1 and FcγRIIB expression, are intricate, involving a network of regulatory pathways encompassing p53, p65 NF-κB, CREB, GATA, and YY1 (Fig. 6-7)

(34). Considering Wip1's known interaction with multiple transcription factors as its substrates (12), we conducted a comparative transcriptomic analysis between T cells and B cells. This exploration unveiled p65 NF- $\kappa$ B and YY1 as the central targets inhibited by Wip1, leading to the down-regulation of PD-1 and Fc $\gamma$ RIIB, consequently promoting lymphocyte activation (Fig. 8). These findings are consistent with the established role of activated p65 NF- $\kappa$ B in fostering the pro-inflammatory environment driving lymphocyte activation to bolster the adaptive immune response. Studies supporting our findings demonstrate that mice lacking Wip1 produce higher levels of pro-inflammatory cytokines—such as IL-1, IL-6, and IL-8—dependent on p65 NF- $\kappa$ B, in their splenic cells. Conversely, it has been evidenced that Wip1 overexpression can dose-dependently reduce p65 NF- $\kappa$ B activation *in vitro* (35). Hence, it is reasonable to speculate that p65 NF- $\kappa$ B primarily stimulates lymphocyte activation upon Wip1 inhibition, rather than directly down-regulating PD-1 and Fc $\gamma$ RIIB expression.

Beyond p65 NF- $\kappa$ B, previous research indicates that silencing YY1 can rejuvenate T cells in patients with chronic HIV infection (36). On the other hand, Fc $\gamma$ RIIB has gained increasing recognition as an Ab checkpoint crucial for enhancing humoral protection<sup>18,37</sup>. Overexpression of YY1 has been shown to enhance the transcription of Fc $\gamma$ RIIB gene in primary and transformed B cells. On the contrary, the loss of the single YY1 binding site at -385 region of promoter sequences (Fig. 6B) due to a single nucleotide polymorphism significantly diminishes Fc $\gamma$ RIIB expression (34). These observations suggest that YY1, rather than p65 NF- $\kappa$ B, primarily influences the transcriptional regulation of PD-1 and Fc $\gamma$ RIIB. Therefore, silencing YY1 appears beneficial for the humoral response by promoting the generation of antiviral Abs for Ab-mediated cytotoxicity. However,



PhosphoSitePlus (v6.7.1.1) notes that both mouse and human YY1 proteins contain numerous potential phosphorylation sites. Mouse YY1 has at least 8 serine residues and 4 threonine residues, while human YY1 has 10 serine residues and 3 threonine residues. Identifying the specific serine or threonine residue requiring phosphorylation to positively regulate the gene expression of PD-1 and FcγRIIB is crucial for the development of specific modulators.

The success of PD-1/PD-L1 checkpoint blockades has significantly expanded their applications in the treatment of cancer patients (38). However, in the context of chronic infections and immune exhaustion, the application of anti-PD-1 and anti-PD-L1 therapies is notably less common. Despite their effectiveness, the high cost of PD-1/PD-L1 blockade therapy presents a substantial barrier to its utilization in chronic infections. Drawing from our findings, we propose the use of a chemical modulator for both PD-1 and FcγRIIB, e.g., CCT007093, to reactivate lymphocytes and enhance immune responses. When used in combination with antiviral drugs, this approach has the potential to significantly augment the efficacy of treatment for patients with chronic infections, especially those suffering from immune exhaustion. Compared to Ab-based PD-1/PD-L1 inhibitors, chemical drugs offer advantages in terms of affordability and safety due to their relatively short half life. Our findings from CCT007093 treatment also highlight several key transcription factors that could be targeted to reduce expression levels of PD-1 and FcγRIIB, either individually or concurrently. Importantly, our data strongly support the concept of dual or multiple targeting to inhibitory receptors to activate both the cytotoxic and humoral arms of the immune system, potentially resulting in superior therapeutic synergism. The optimal strategy would involve the use of small molecules to block the action of immune

checkpoint receptors, combining them with antiviral treatments, and identifying the novel, safer and more effective immunotherapeutic targets.

Of importance, our findings also have implications for the application of chemical checkpoint inhibitors for the treatment of cancer patients. Based on our data, we reason that CCT007093 may not be an effective treatment for cancer. This speculation primarily stems from the well-established role of p65 NF- $\kappa$ B in promoting tumor growth (39). Therefore, it is not surprising to know that CCT007093 treatment has shown inconsistent therapeutic benefits in different types of cancers with wild-type p53 (40). Nevertheless, our findings suggest that YY1 could be a more suitable target for enhancing T cell cytotoxicity and inhibiting tumor growth. YY1 is a ubiquitously distributed transcription factor belonging to the GLI-Kruppel class of zinc finger proteins. Its role as a transcriptional repressor or activator varies depending on the cellular context (41). In cancer cells, YY1 modulates immune resistance by enhancing PD-L1 expression (42) and promotes cancer metastasis (43). These findings highlight YY1 as a more promising target for chemical drugs to alleviate immune exhaustion caused by cancer cells. As mentioned earlier, blocking Fc $\gamma$ RIIB can enhance the production of anti-tumor Abs, which is crucial for enhancing cancer immunotherapy (37).

In summary, we present a novel strategy to address immune exhaustion of lymphocytes and demonstrate its feasibility. CCT007093 and its derivatives emerge as promising candidate compounds for treating immune exhaustion in infectious diseases. Moreover, the exploration and characterization of chemical compounds to reduce the expression levels of inhibitory receptors hold significant potential for expanding therapeutic options in cancer patients. Furthermore, the critical role of Fc $\gamma$ RIIB in

enhancing humoral protection against infection and tumor appears to be under-recognized. Therefore, future research efforts should consider the inclusion of FcγRIIB in the development of new checkpoint inhibitors. This becomes particularly significant when safeguarding against acute bacterial and viral infections is essential, as we and other researchers have recently affirmed (18, 44).

### **Acknowledgements**

This work was supported by Taiwan National Science and Technology Council (NSTC) grants NSC 102-2633-B-002-001 and MOST 103-2633-B-002-001, and National Health Research Institutes (NHRI) grant NHRI-EX109-10932SI. We would like to express our gratitude to the First, Second, and Seven Core Laboratories of National Taiwan University Hospital and the Laboratory Animal Center of National Taiwan University College of Medicine for their invaluable support throughout the study. We also thank the staff of the Sequencing Core, Department of Medical Research, National Taiwan University Hospital for excellent technical supports.

### **Declaration of competing interests**

The authors declare that they have no competing interests.

### **Author contributions**

SJT conceived the study and obtained funding support. YSY, WTC, YFL, HYW and SJT contributed to the development of methodology, performed experiments, and

acquired and interpreted the data. CLH conducted bioinformatic analysis, and CLH and SJT interpreted the results. YSY, CLH, IK and SJT drafted the manuscript. SJT designed and supervised the work, and provided administrative, technical, or material supports. All authors approved the final version of the manuscript.

## References

1. E.J. Wherry, M. Kurachi. Molecular and cellular insights into T cell exhaustion. *Nat Rev Immunol.* **15**, 486-499 (2015).
2. K. Roe. NK-cell exhaustion, B-cell exhaustion and T-cell exhaustion-the differences and similarities. *Immunology.* **166**, 155-168 (2022).
3. G. Peng. *et al.*, PD-1 upregulation is associated with HBV-specific T cell dysfunction in chronic hepatitis B patients. *Mol Immunol.* **45**, 963-970 (2008).
4. Y. Dong *et al.*, CD4<sup>+</sup> T cell exhaustion revealed by high PD-1 and LAG-3 expression and the loss of helper T cell function in chronic hepatitis B. *BMC Immunol.* **20**, 27 (2019).
5. L. Kardava *et al.*, Attenuation of HIV-associated human B cell exhaustion by siRNA downregulation of inhibitory receptors. *J Clin Invest.* **121**, 2614-2624 (2011).
6. C.L. Day *et al.*, PD-1 expression on HIV-specific T cells is associated with T-cell exhaustion and disease progression. *Nature.* **443**, 350-354 (2006).
7. P. Fisicaro *et al.*, Antiviral intrahepatic T-cell responses can be restored by blocking programmed death-1 pathway in chronic hepatitis B. *Gastroenterology.* **138**, 682-693 (2010).

8. H.T. Tzeng *et al.*, PD-1 blockage reverses immune dysfunction and hepatitis B viral persistence in a mouse animal model. *PLoS One*. **7**, e39179 (2012).
9. C. Gubser, C. Chiu, S.R. Lewin, T.A. Rasmussen. Immune checkpoint blockade in HIV. *EBioMedicine*. **76**, 103840 (2022).
10. L. Salimzadeh *et al.*, PD-1 blockade partially recovers dysfunctional virus-specific B cells in chronic hepatitis B infection. *J Clin Invest*. **128**, 4573-4587 (2018).
11. S.J. Chen. Pharmacological modulation and its mechanism on the expression of the inhibitory Fc receptor in B cells as a therapeutic for systemic lupus erythematosus. *Master Thesis*. (2012).
12. Y.H. Zhu, D.V. Bulavin. Wip1-dependent signaling pathways in health and diseases. *Prog Mol Biol Transl Sci*. **106**, 307-325 (2012).
13. L.R. Huang, H.L. Wu, P.J. Chen, D.S. Chen. An immunocompetent mouse model for the tolerance of human chronic hepatitis B virus infection. *Proc Natl Acad Sci U S A*. **103**, 17862-17867 (2006).
14. J.P. Jhou *et al.*, The lupus-associated Fc $\gamma$  Receptor IIb-I232T polymorphism results in impairment in the negative selection of low-affinity germinal center B cells via c-Abl in mice. *Arthritis Rheumatol*. **70**, 1866-1878 (2018).
15. T.C. Tseng *et al.*, Dual immuno-renal targeting of 7-benzylidenenaltrexone alleviates lupus nephritis via Fc $\gamma$ RIIB and HO-1. *J Mol Med (Berl)*. **96**, 413-425 (2018).
16. S.J. Tzeng. The isolation, differentiation, and quantification of human antibody-secreting B cells from blood: ELISpot as a functional readout of humoral immunity. *J Vis Exp*. **118**, 54582 (2016).

17. G. Klein *et al.*, Continuous lymphoid cell lines with characteristics of B cells (bone-marrow-derived), lacking the Epstein-Barr virus genome and derived from three human lymphomas. *Proc Natl Acad Sci U S A.* **71**, 3283-3286 (1974).
18. Y.H. Wu *et al.*, FcγRIIB modulates splenic germinal center response against immune subversion during acute influenza A virus infection. *J Microbiol Immunol Infect.* S1684-1182(23)00213-X. (2023). doi: 10.1016/j.jmii.2023.11.007.
19. A. Dobin *et al.*, STAR: ultrafast universal RNA-seq aligner. *Bioinformatics.* **29**, 15-21 (2013).
20. M.D. Robinson, D.J. McCarthy, G.K. Smyth. edgeR: a Bioconductor package for differential expression analysis of digital gene expression data. *Bioinformatics.* **26**, 139-140 (2010).
21. S. Tarazona *et al.*, Conesa A. Data quality aware analysis of differential expression in RNA-seq with NOISeq R/Bioc package. *Nucleic Acids Res.* **43**, e140 (2015).
22. T. Wu *et al.*, clusterProfiler 4.0: A universal enrichment tool for interpreting omics data. *Innovation (Camb).* **2**, 100141 (2021).
23. A. Liberzon *et al.*, Molecular signatures database (MSigDB) 3.0. *Bioinformatics.* **27**, 1739-1740 (2011).
24. Y.J. Lin *et al.*, Hepatitis B virus core antigen determines viral persistence in a C57BL/6 mouse model. *Proc Natl Acad Sci U S A.* **107**, 9340-9345 (2010).
25. C. Boni *et al.*, Characterization of hepatitis B virus (HBV)-specific T-cell dysfunction in chronic HBV infection. *J Virol.* **81**, 4215-4225 (2007).
26. S.J. Tzeng, W.Y. Li, H.Y. Wang. FcγRIIB mediates antigen-independent inhibition on human B lymphocytes through Btk and p38 MAPK. *J Biomed Sci.* **22**, 87 (2015).

27. A.A. Ambegaonkar *et al.*, Expression of inhibitory receptors by B cells in chronic human infectious diseases restricts responses to membrane-associated antigens. *Sci Adv.* **6**, eaba6493 (2020).
28. J.P. Jhou *et al.*, Upregulation of FcγRIIB by resveratrol via NF-κB activation reduces B-cell numbers and ameliorates lupus. *Exp Mol Med.* **49**, e381 (2017).
29. T.J. Liang *et al.*, Present and future therapies of hepatitis B: From discovery to cure. *Hepatology.* **62**, 1893-1908 (2015).
30. Y. Cai, W. Yin. The multiple functions of B cells in chronic HBV infection. *Front Immunol.* **11**, 582292 (2020).
31. Y. Kidani *et al.*, Sterol regulatory element-binding proteins are essential for the metabolic programming of effector T cells and adaptive immunity. *Nat Immunol.* **14**, 489-499 (2013).
32. W. Luo *et al.*, SREBP signaling is essential for effective B cell responses. *Nat Immunol.* **24**, 337-348 (2023).
33. J.W.M. Fowler, R. Zhang, B. Tao, N.E. Boutagy, W.C. Sessa. Inflammatory stress signaling via NF-κB alters accessible cholesterol to upregulate SREBP2 transcriptional activity in endothelial cells. *Elife.* **11**, e79529 (2022).
34. K. Su *et al.*, A promoter haplotype of the immunoreceptor tyrosine-based inhibitory motif-bearing FcγRIIb alters receptor expression and associates with autoimmunity. II. Differential binding of GATA4 and Yin-Yang1 transcription factors and correlated receptor expression and function. *J Immunol.* **172**, 7192-199 (2004).
35. J. Chew *et al.*, WIP1 phosphatase is a negative regulator of NF-kappaB signalling. *Nat Cell Biol.* **11**, 659-666 (2009).

36. M.Y. Balkhi, G. Wittmann, F. Xiong, R.P. Junghans. YY1 upregulates checkpoint receptors and downregulates type I cytokines in exhausted, chronically stimulated human T cells. *iScience*. **2**, 105-122 (2018).
37. I. Teige, L. Mårtensson, B.L. Frendéus. Targeting the antibody checkpoints to enhance cancer immunotherapy-focus on FcγRIIB. *Front Immunol*. **10**, 481 (2019).
38. T. Okazaki, S. Chikuma, Y. Iwai, S. Fagarasan, T. Honjo. A rheostat for immune responses: the unique properties of PD-1 and their advantages for clinical application. *Nat Immunol*. **14**, 1212-1218 (2013).
39. K. Taniguchi, M. Karin. NF-κB, inflammation, immunity and cancer: coming of age. *Nat Rev Immunol*. **18**, 309-324 (2018).
40. W. Deng *et al.*, The role of PPM1D in cancer and advances in studies of its inhibitors. *Biomed Pharmacother*. **125**, 109956 (2020).
41. R.P. Hyde-DeRuyscher, E. Jennings, T. Shenk. DNA binding sites for the transcriptional activator/repressor YY1. *Nucleic Acids Res*. **23**, 4457-4465 (1995).
42. E. Hays, B. Bonavida. YY1 regulates cancer cell immune resistance by modulating PD-L1 expression. *Drug Resist Updat*. **43**, 10-28 (2019).
43. W. Wang, D. Li, G. Sui. YY1 is an inducer of cancer metastasis. *Crit Rev Oncog*. **22**, 1-11 (2017).
44. M.R. Clatworthy, K.G. Smith. FcγRIIb balances efficient pathogen clearance and the cytokine-mediated consequences of sepsis. *J Exp Med*. **199**, 717-723 (2004).



## Figure Legends

**Figure 1.** CCT007093 treatment markedly reduced serum HBsAg levels in chronic HBV-infected mice. (A) Schematic illustration delineating the induction of immune exhaustion through chronic HBV infection (detailed in Methods) and the treatment protocols involving either vehicle (PBS, represented by circles, n=6) or CCT007093 (displayed as squares, n=8). (B) Male mice underwent an 8-week protocol to confirm the successful induction of immune exhaustion before treatment initiation. Serum HBsAg levels were measured before and after a 2-week treatment period using either vehicle or CCT007093. Mouse serum samples were diluted threefold for HBsAg quantification.

**Figure 2.** CCT007093 attenuated PD-1 and FcγRIIB expression in circulating lymphocytes of chronic HBV-infected mice. (A) Flow cytometry data (left) illustrating PD-1<sup>+/hi</sup>CD4<sup>+</sup> T cells in peripheral blood from immune exhausted HBV-infected mice treated with either vehicle or CCT007093. The middle section displays the percentages of PD-1<sup>+/hi</sup>CD4<sup>+</sup> T cells, and the right section indicates mean fluorescence intensity (MFI) of PD-1 expression levels in these T cells for mice treated with vehicle (solid circles in white bar, n=6) or CCT007093 (solid squares in grey bar, n=8-9). Data were analyzed using FlowJo software. (B) Flow cytometry analysis (left) demonstrating circulating PD-1<sup>+/hi</sup>CD8<sup>+</sup> T cells from HBV-infected mice with immune exhausted treated with either vehicle or CCT007093. The middle panel indicates the percentages of PD-1<sup>+/hi</sup>CD8<sup>+</sup> T cells, while the right panel illustrates the MFI of PD-1 expression levels in these T cells for mice treated with vehicle (solid circles, n=6) or CCT007093 (solid squares, n=7). (C) Flow cytometry data (left) showing circulating PD-1<sup>+/hi</sup>CD19<sup>+</sup> B cells from HBV-infected mice with immune

exhaustion treated with either vehicle or CCT007093. The middle section represents the percentages of PD-1<sup>+/hi</sup>CD19<sup>+</sup> B cells, and the right section exhibits the MFI of PD-1 expression levels for mice treated with vehicle (solid circles, n=5) or CCT007093 (solid squares, n=9). (D) Flow cytometry analysis (left) illustrating circulating FcγRIIB<sup>+/hi</sup>CD19<sup>+</sup> B cells from HBV-infected mice with immune exhaustion treated with either vehicle or CCT007093. The middle section shows the percentages of FcγRIIB<sup>+/hi</sup>CD19<sup>+</sup> B cells, while the right section demonstrates the MFI of FcγRIIB expression levels in these B cells for mice treated with vehicle (solid circles, n=5) or CCT007093 (solid squares, n=9). All data were analyzed using FlowJo software. The statistical significance was determined using the two-tailed unpaired *t*-test, and significance levels are indicated as follows: \**p* < 0.05, \*\**p* < 0.01, \*\*\**p* < 0.001. These notations are consistently used throughout the figures.

**Figure 3.** CCT007093 reduced PD-1 and FcγRIIB expression in splenic lymphocytes of chronic HBV-infected mice. (A) Flow cytometric analysis illustrating PD-1<sup>+/hi</sup>CD4<sup>+</sup> (left upper) and PD-1<sup>+/hi</sup>CD8<sup>+</sup> T cells (left lower) in splenocytes from immune exhausted HBV-infected mice treated with either vehicle or CCT007093. Quantification results showed the percentages of PD-1<sup>+/hi</sup>CD4<sup>+</sup> (upper middle) and PD-1<sup>+/hi</sup>CD8<sup>+</sup> (lower middle) T cells, as well as the MFI of PD-1 expression levels for PD-1<sup>+/hi</sup>CD4<sup>+</sup> (upper right) and PD-1<sup>+/hi</sup>CD8<sup>+</sup> (lower right) T cells in mice treated with vehicle (solid circles in white bar, n=5-8) or CCT007093 (solid squares in grey bar, n=5-10), respectively. (B) Flow cytometric analysis depicting PD-1<sup>+/hi</sup>CD127<sup>lo</sup>CD4<sup>+</sup> (left upper) and PD-1<sup>+/hi</sup>CD127<sup>lo</sup>CD8<sup>+</sup> T cells (left lower) in splenocytes from immune exhausted HBV-infected mice treated with either vehicle or CCT007093. Quantification results showed the percentages of PD-1<sup>+/hi</sup>CD127<sup>lo</sup>CD4<sup>+</sup>

(upper middle) and PD-1<sup>+hi</sup>CD127<sup>lo</sup>CD8<sup>+</sup> (lower middle) T cells, along with the MFI of PD-1 expression levels for PD-1<sup>+hi</sup>CD127<sup>lo</sup>CD4<sup>+</sup> (right upper) and PD-1<sup>+hi</sup>CD127<sup>lo</sup>CD8<sup>+</sup> (right lower) T cells in mice treated with vehicle (solid circles, n=4-5) or CCT007093 (solid squares, n=5). (C) Flow cytometric analysis representing PD-1<sup>+hi</sup>CD19<sup>+</sup> (left upper) and FcγRIIB<sup>+hi</sup>CD19<sup>+</sup> B cells (left lower) in splenocytes from immune exhausted HBV-infected mice treated with either vehicle or CCT007093. Quantification results disclosed the percentages of PD-1<sup>+hi</sup>CD19<sup>+</sup> (upper middle) and FcγRIIB<sup>+hi</sup>CD19<sup>+</sup> (lower middle) B cells, as well as the MFI of PD-1 expression levels for PD-1<sup>+hi</sup>CD19<sup>+</sup> (upper right) and FcγRIIB<sup>+hi</sup>CD19<sup>+</sup> (lower right) B cells in mice treated with vehicle (solid circles, n=6-9) or CCT007093 (solid squares, n=8-11). Statistical significance: \**p* < 0.05, \*\**p* < 0.01, \*\*\**p* < 0.001.

**Figure 4.** CCT007093 downregulated PD-1 and FcγRIIB expression levels in intrahepatic lymphocytes of immune exhausted HBV-infected mice. (A) representative flow cytometric analysis depicting the expression levels of PD-1 in intrahepatic CD4 T cells (upper left) and CD8 T cells (lower left) in HBV-infected mice treated with vehicle or CCT007093. The middle panels displayed quantification results of CD4 (upper) and CD8 (lower) T cells in bar graphs (vehicle in white bar; CCT007093 in grey bar), while the right panels illustrated the percentages of PD-1<sup>+hi</sup>CD4<sup>+</sup> (upper, n=5-9) and PD-1<sup>+hi</sup>CD8<sup>+</sup> (lower, n=5-9) intrahepatic T cells, respectively. (B) Flow cytometric analysis (left) and quantification (right) showing the percentages of PD-1<sup>+hi</sup>CD127<sup>low</sup>CD4<sup>+</sup> (upper, n=4-6) and PD-1<sup>+hi</sup>CD127<sup>low</sup>CD8<sup>+</sup> T cells (lower, n=4) in HBV-infected mice treated with vehicle or CCT007093. (C) Flow cytometric analysis (left) of the expression levels of PD-1 (upper)

and FcγRIIB (lower) in intrahepatic CD19<sup>+</sup> B cells in HBV-infected mice treated with vehicle or CCT007093. The middle panels exhibited quantification results of PD-1<sup>+</sup> (upper) and FcγRIIB<sup>+</sup> (lower) B cells in bar graphs, while the right panels illustrated the percentages of intrahepatic PD-1<sup>+/hi</sup> (upper) and FcγRIIB<sup>+/hi</sup> CD19<sup>+</sup> B cells, respectively, in HBV-infected mice treated with vehicle (solid circles, n=3-8) or CCT007093 (solid squares, n=5-10). Statistical significance: \**p* < 0.05, \*\**p* < 0.01, \*\*\**p* < 0.001.

**Figure 5.** *Ex vivo* enhanced cytotoxicity and Ab production of intrahepatic lymphocytes from CCT007093 treated HBV-infected mice. Quantification of flow cytometric analysis showing the percentage of intrahepatic IFN-γ-producing T cells, including (A) CD4 (n=4-5) and (B) CD8 (n=4) T cells, isolated from mice treated with either vehicle or CCT007093. The T cells were subjected to *ex vivo* stimulation for 3 hr. Additionally, (C) The percentages of anti-HBsAg (left, n=4) and anti-HBcAg (right, n=5-6) antibody-secreting cells (ASCs) were quantified using ELISPOT assays and depicted in bar graphs to compare between mice treated with vehicle or CCT007093 during immune exhaustion induced by HBV infection. Statistical significance: \**p* < 0.05, \*\**p* < 0.01, \*\*\**p* < 0.001.

**Figure 6.** Reduction of PD-1 and FcγRIIB promoter transcriptional activities by CCT007093 treatment in BJAB B cells. (A) Illustration of predicted transcription factor binding sites within the -2,200 bp of the PD-1 promoter and (B) the -1,522 bp of FcγRIIB promoter employing TRANSFAC. (C) BJAB B cells (1-2×10<sup>6</sup>) were transiently co-transfected with either the -926 bp, -1075 bp, -1636 bp or -2200 bp promoter sequences of PD-1 pGL3 and renilla luciferase plasmids (pRL-TK). This transfection was conducted

in the absence or presence of 2 or 5  $\mu$ M CCT007093 for 24 hr to assess their promoter activities. (D) BJAB B cells were transiently co-transfected with either the –1522 bp or the –600 bp promoter sequences of Fc $\gamma$ RIIB pGL3 and renilla pRL-TK plasmids in the absence or presence of 2 or 5  $\mu$ M CCT007093 to evaluate the promoter activities linked to Fc $\gamma$ RIIB.

**Figure 7.** Impact of CCT007093 treatment on transcriptional regulators of PD-1 and Fc $\gamma$ RIIB genes. (A) BJAB B cells ( $1 \times 10^6$ ) were subjected to treatment with CCT007093 at concentrations of 0, 5, 10, or 25  $\mu$ M for durations of 15 min, 1 hr, and 6 hr, respectively. After treatment, cells were harvested and lysed for western blotting, aiming to quantify the levels of PD-1, Fc $\gamma$ RIIB, Wip1, p53, p-p53 (S15), p65 NF- $\kappa$ B, p-p65 (S536), and  $\beta$ -actin. As a standard for quantification,  $\beta$ -actin was employed as an internal control. (B) HEK293T cells ( $2.4 \times 10^5$ /ml) were transfected with myc-tagged Wip1 constructs, both with or without YY1 constructs. Subsequent to 24 hr of transfection, the cells underwent treatment with 25  $\mu$ M CCT007093 for 1 hr, followed by harvesting for cell lysates. For immunoprecipitation, cell lysates were utilized with anti-Wip1 or anti-YY1 Abs, and immunoblotting was carried out utilizing the designated Abs.

**Figure 8.** Comparative analysis of transcriptomics between vehicle and CCT007093 treated Jurkat T and BJAB B cells. Jurkat T cells and BJAB B cells ( $1 \times 10^6$ /ml) were treated with either vehicle (DMSO) or 25  $\mu$ M CCT007093 for 16 hr. Following this, total RNAs were extracted for RNA-sequencing. The data analysis resulted in the following components: (A) Venn diagram illustrating the number of genes commonly up- (left) and down-regulated (right) in both Jurkat and BJAB cells. (B) A heatmap displaying the

expression patterns of genes commonly up- and down-regulated in both Jurkat and BJAB cells. (C) Functional regulatory networks associated with inflammatory pathways were constructed based on genes commonly up- and down-regulated in both Jurkat and BJAB cells, analyzed using IPA. (D) Deciphering transcription factor (TF) activity in response to CCT007093 treatment. A Venn diagram was created to illustrate the number of TFs with commonly activated (top) and suppressed (bottom) transcriptional activity in both Jurkat and BJAB cells following CCT007093 treatment. (E) GSEA plots illustrate the expression of genes targeted by p65 NF- $\kappa$ B (top) and YY1 (bottom) in BJAB and Jurkat cells treated with CCT007093 compared to the vehicle.  $P < 0.05$  indicates statistical significance.

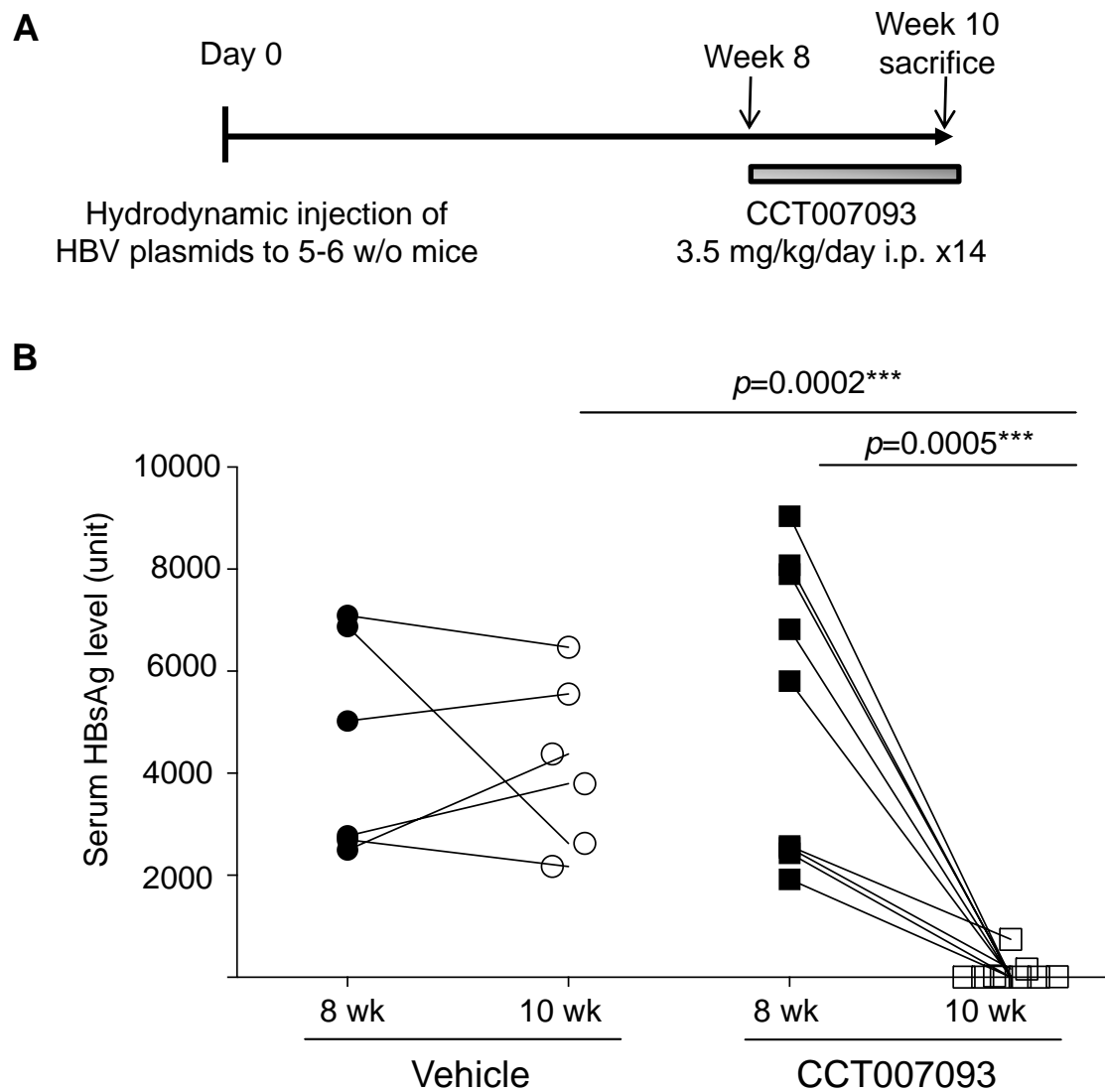
### **Supplementary Information**

**Supplementary Table 1.** Differentially expressed genes in Jurkat and BJAB cells in response to vehicle or CCT007093. This supplementary table provides a list of genes that exhibit differential expression in the comparisons between vehicle (DMSO) versus CCT007093 treated Jurkat T and BJAB B cells. These gene lists were employed to construct the Venn diagram shown in Fig. 8A. Log2FC denotes log2-transformed fold-change values.

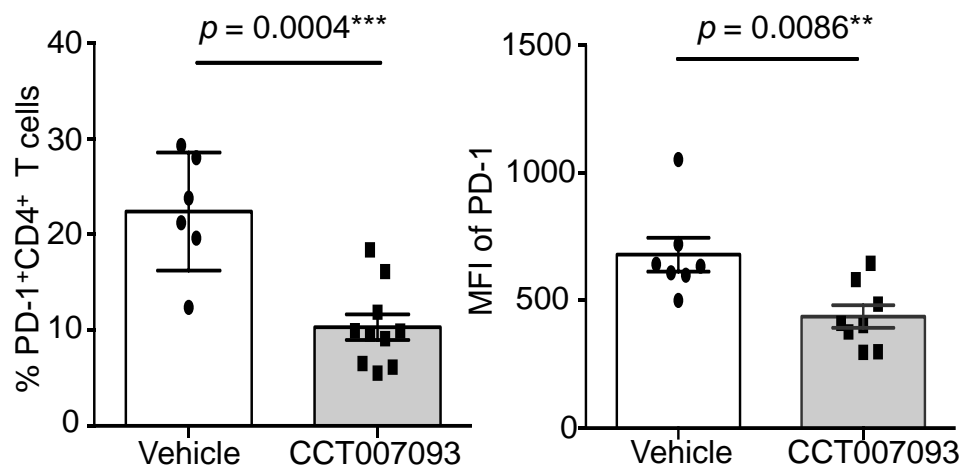
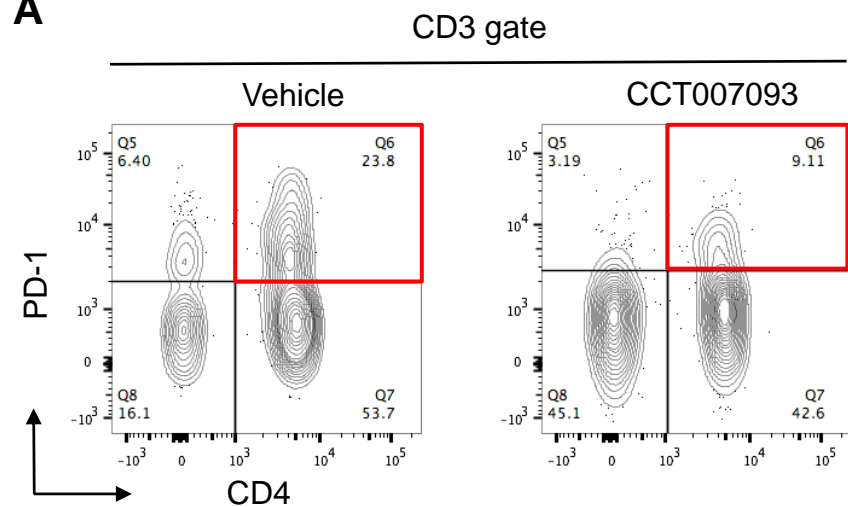
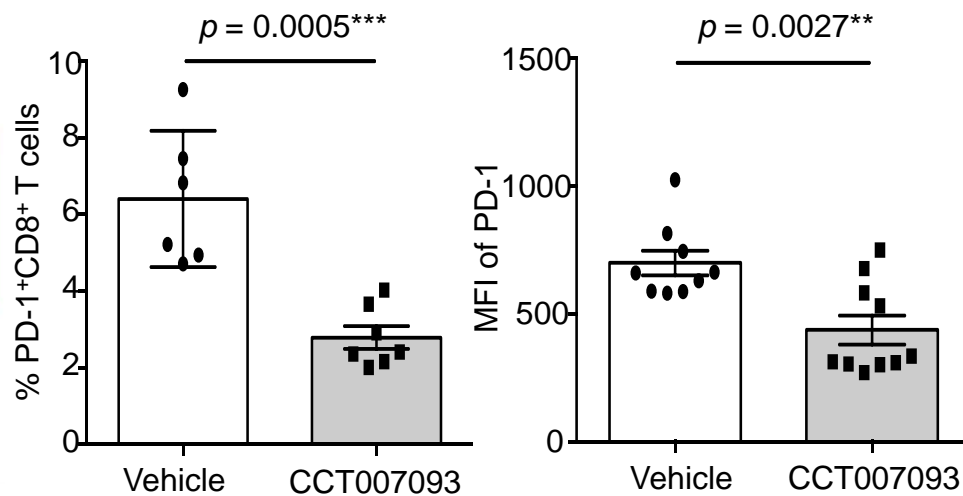
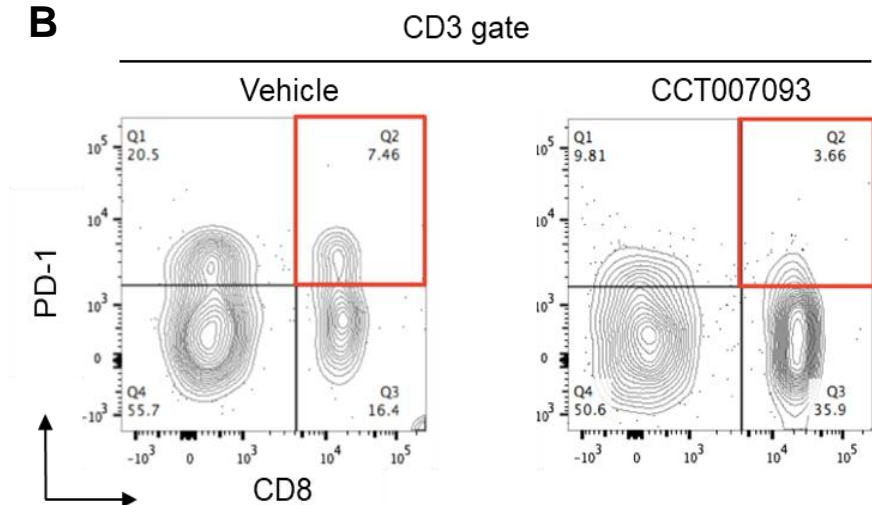
**Supplementary Table 2.** Transcription factor targets showing enrichment in response to CCT007093 treatment in Jurkat or BJAB cells. The list of transcription factor targets was sourced from MSigDB's c7-tft category, and the enrichment analysis was conducted using GSEA.

**Supplementary Fig. 1.** GSEA plots of genes targeted by TFs in cells treated with CCT007093 compared to vehicle. List of TFs showing significant differences in GSEA plots between cells treated with vehicle versus CCT007093. GSEA plots illustrating the expression of genes targeted by relevant (Fig. 6 and 8) and significant TFs in Jurkat T and BJAB B cells treated with CCT007093 compared to vehicle. The list includes: (A) Tumor protein 53 (TP53), (B) Cyclic AMP-responsive element-binding protein 1 (CREB1), (C) Androgen receptor (AR), (D) Zinc finger protein 589 (ZNF589), (E) Nuclear factor Y (NF-Y, also known as CCAAT-binding factor (CBF)), (F) Thyroid hormone receptor  $\alpha$  (THRA), (G) Activator protein 1 (AP-1), (H) Mitogen-activated protein kinase 3 (MAPK3, also known as p44 MAPK and ERK1), (I) Serum response factor (SRF), (J) General transcription factor IIE subunit 2 (GTF2E2), and (K) Double-stranded RNA-specific endoribonuclease (DROSHA) genes.  $p < 0.05$  indicates statistical significance.

**Fig. 1**

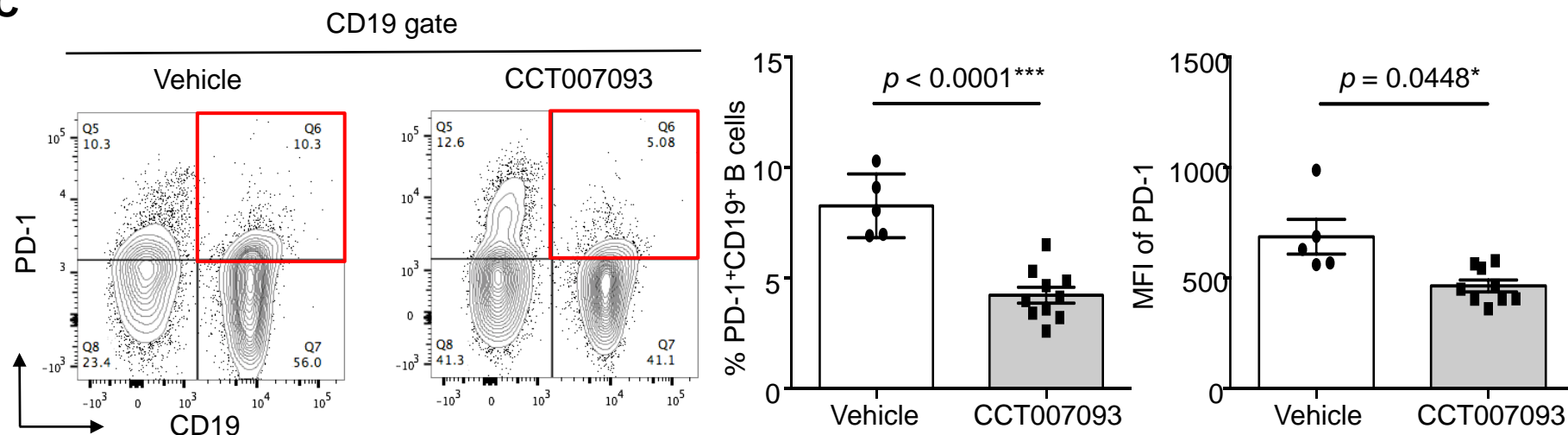




**Fig. 2****A****B**

**Fig. 2**

**C**



**D**

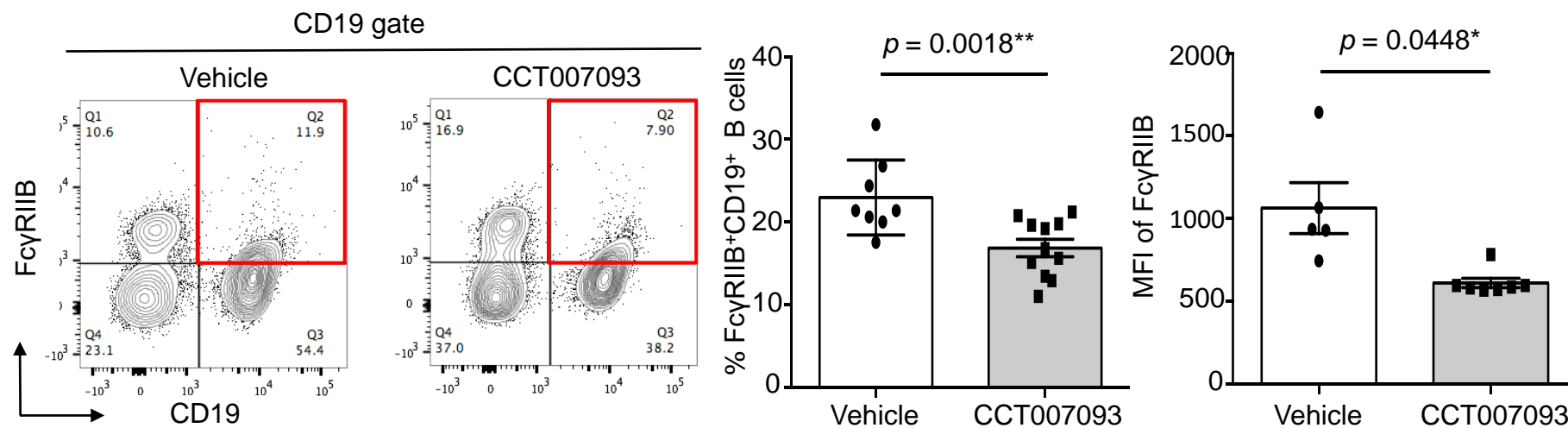


**Fig. 3**

**A**

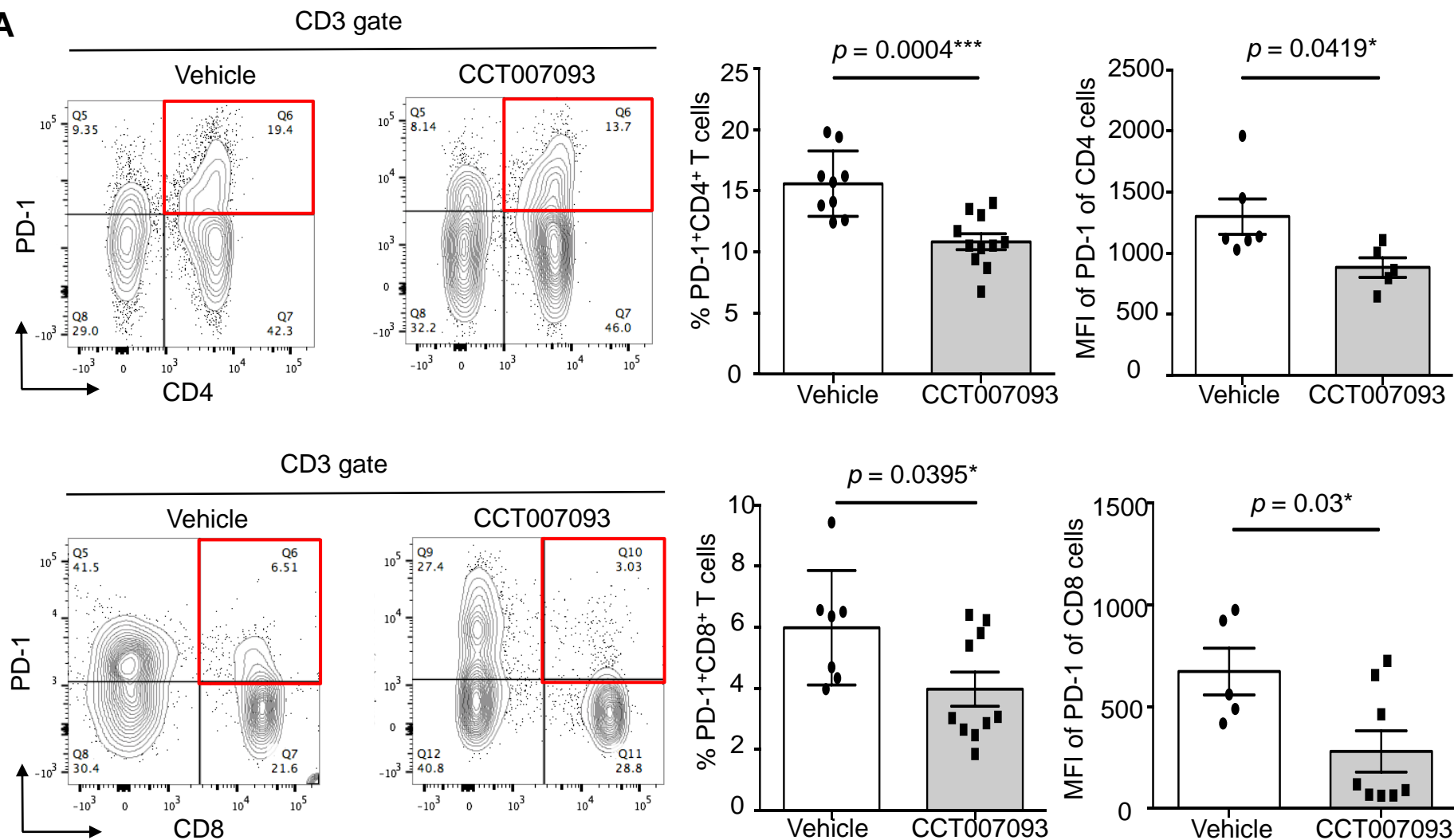


**Fig. 3**

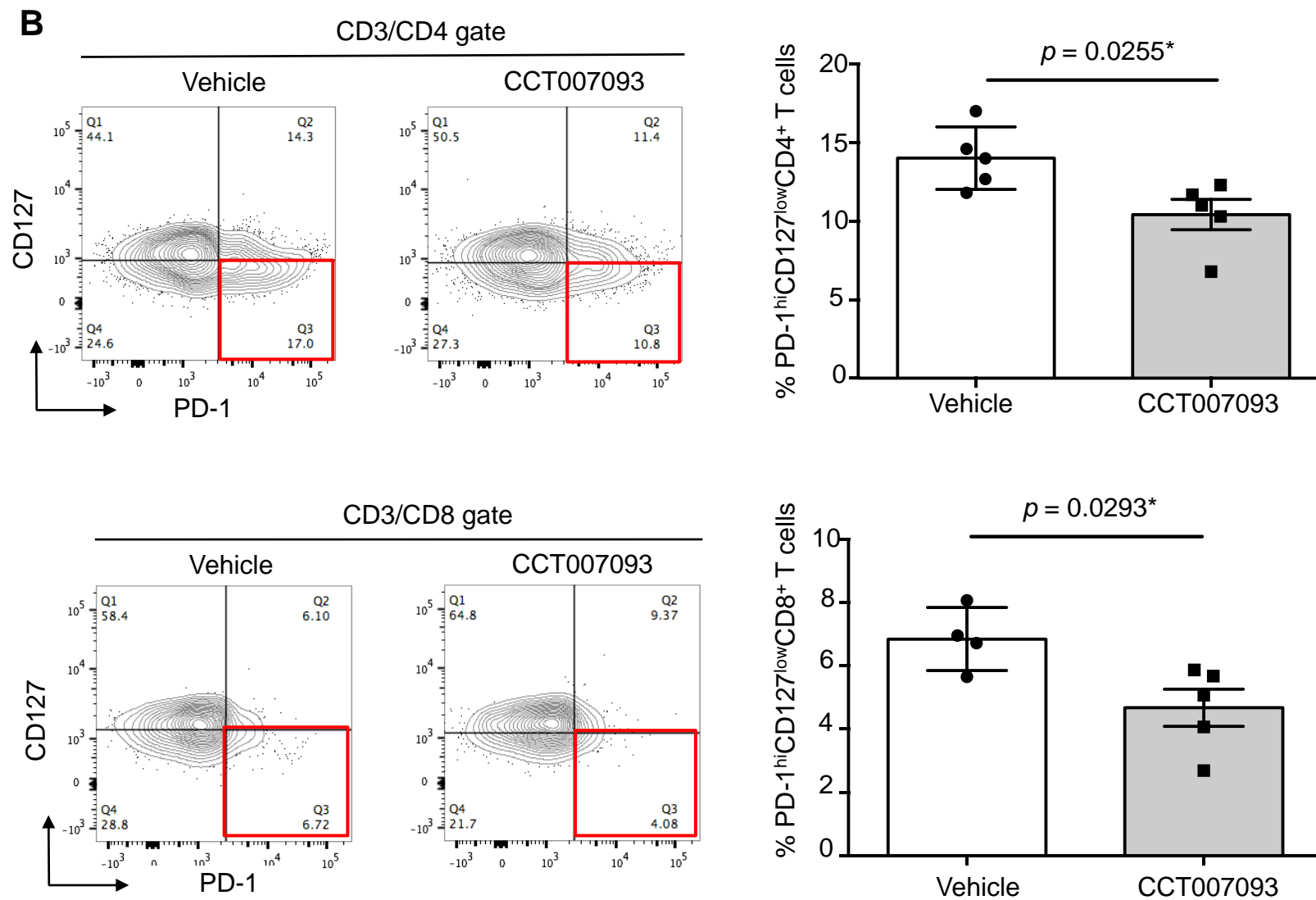


**Fig. 3**

**C**

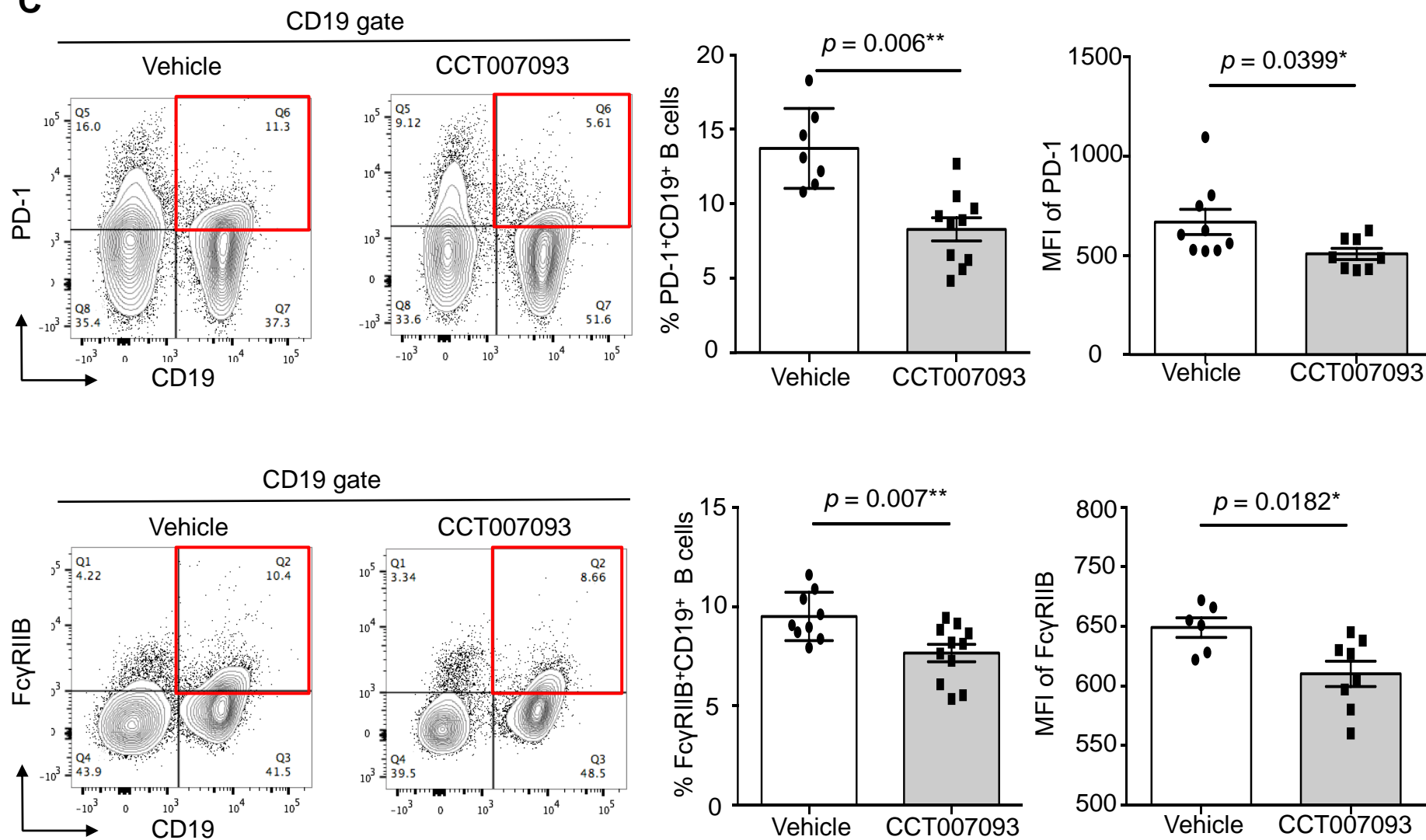


**Fig. 4**

**A**

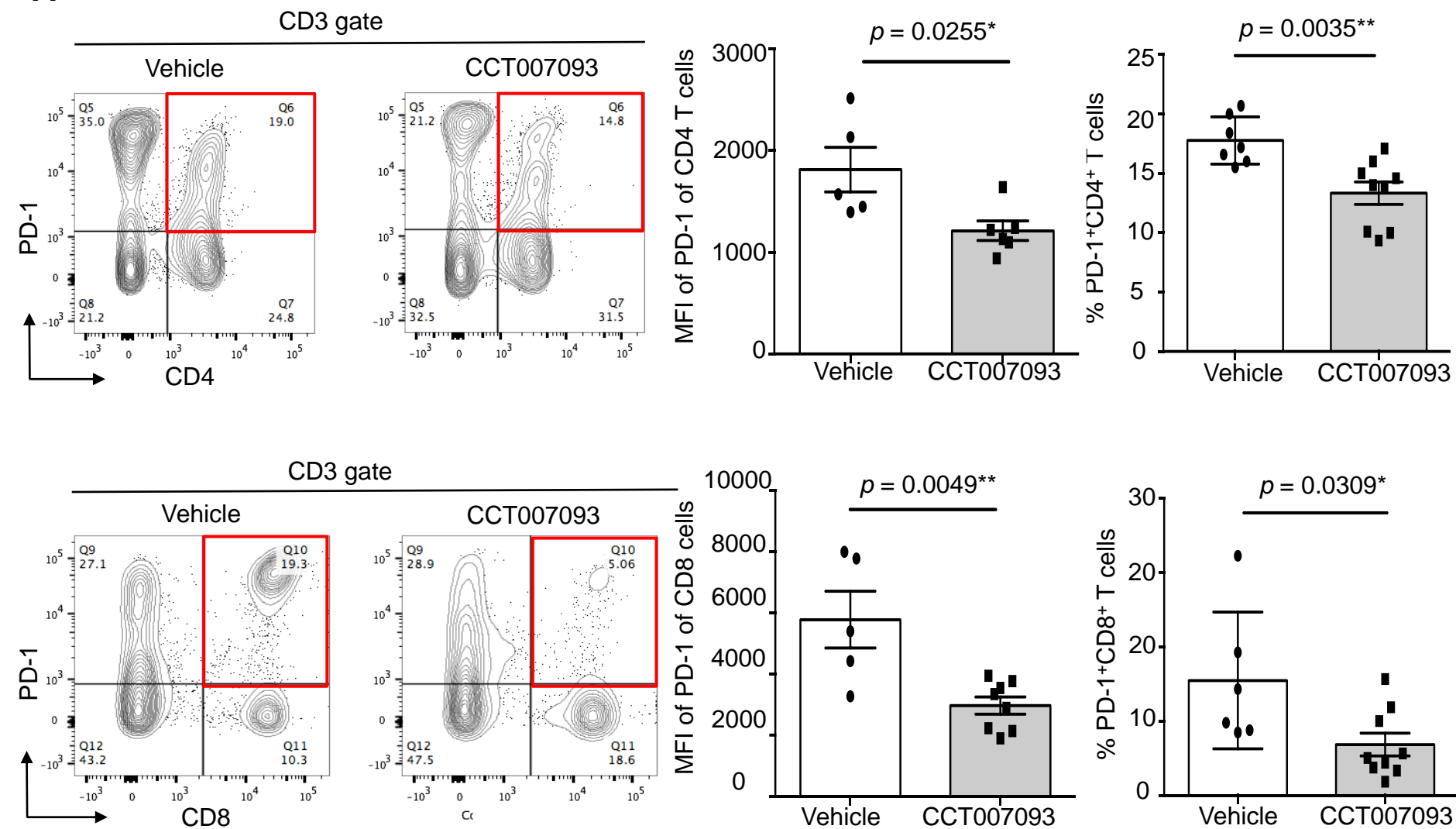


**Fig. 4**

**B**

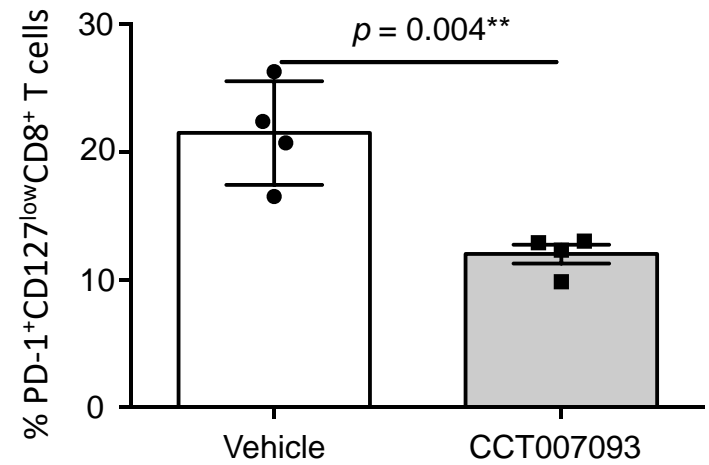
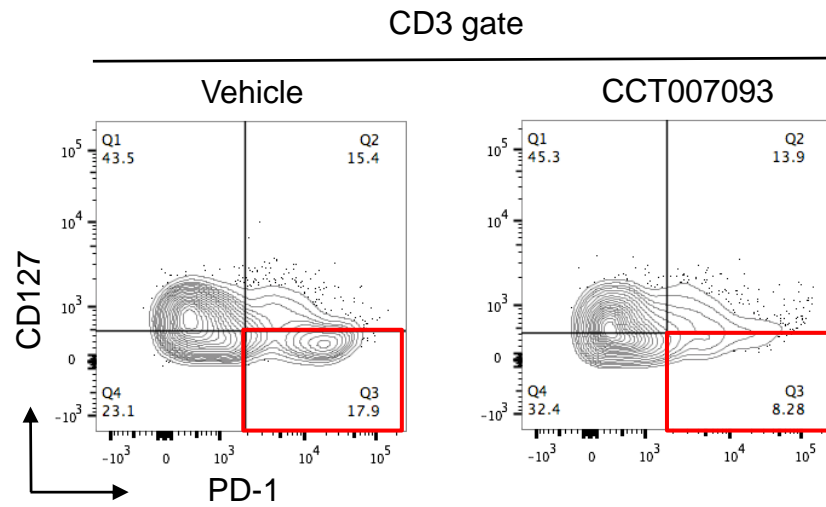
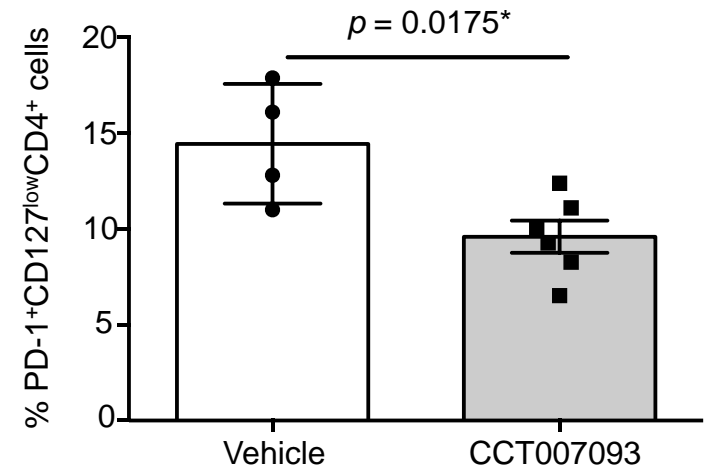
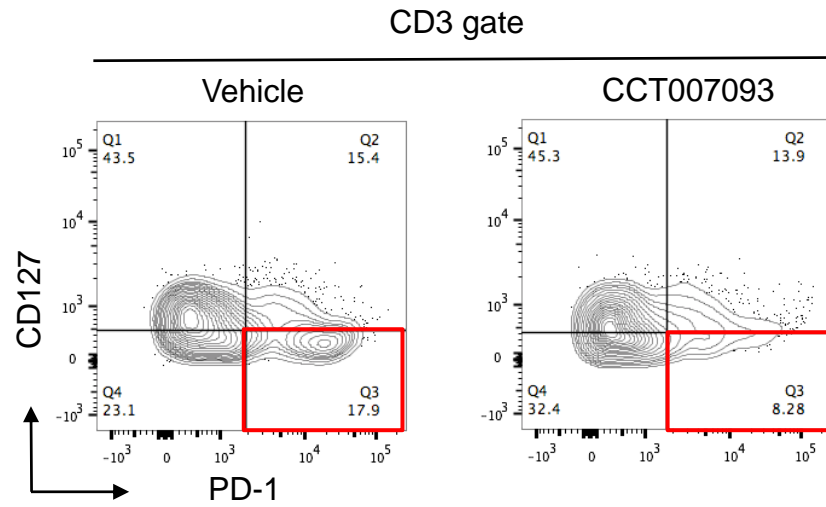
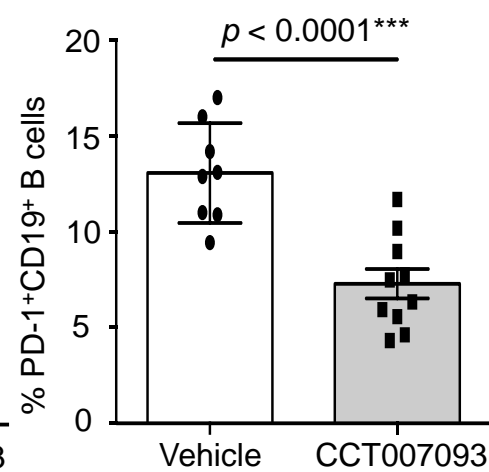
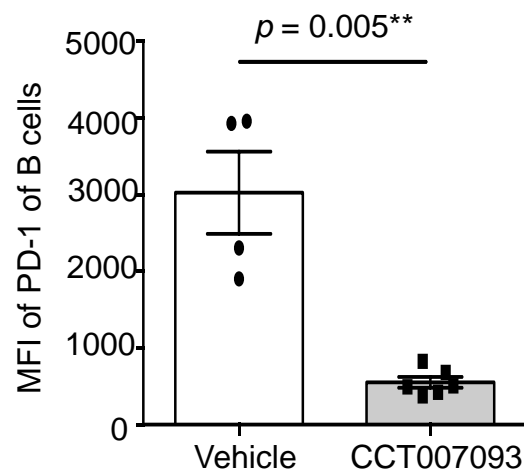
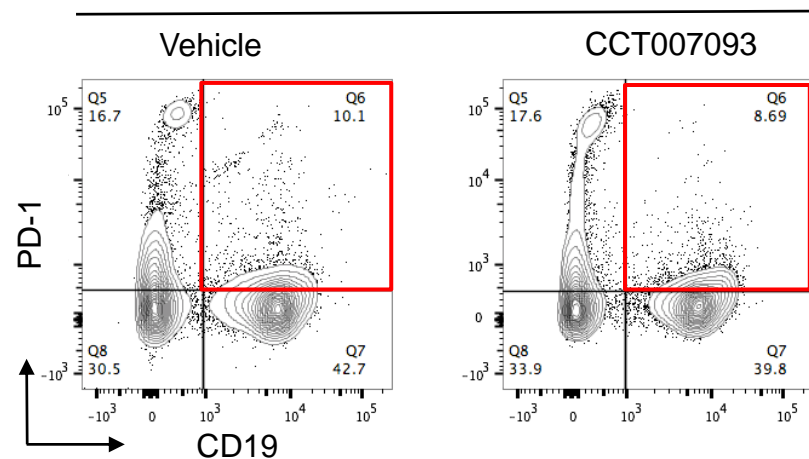


**Fig. 4**

**C**

CD19 gate



CD19 gate

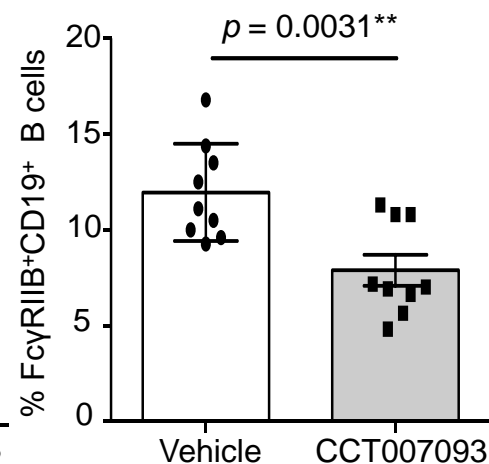
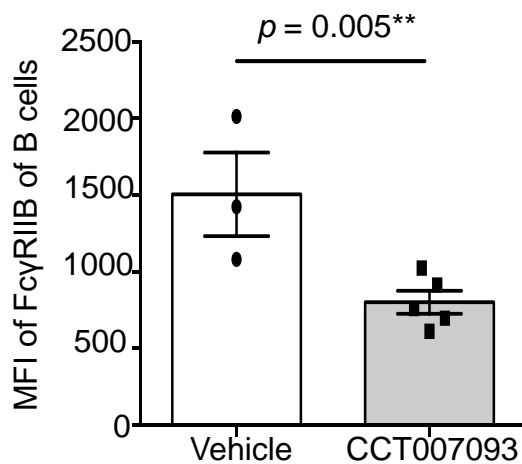
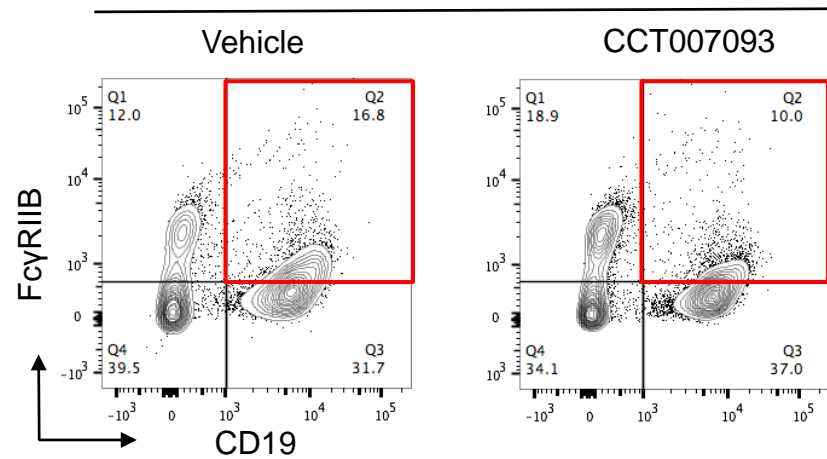
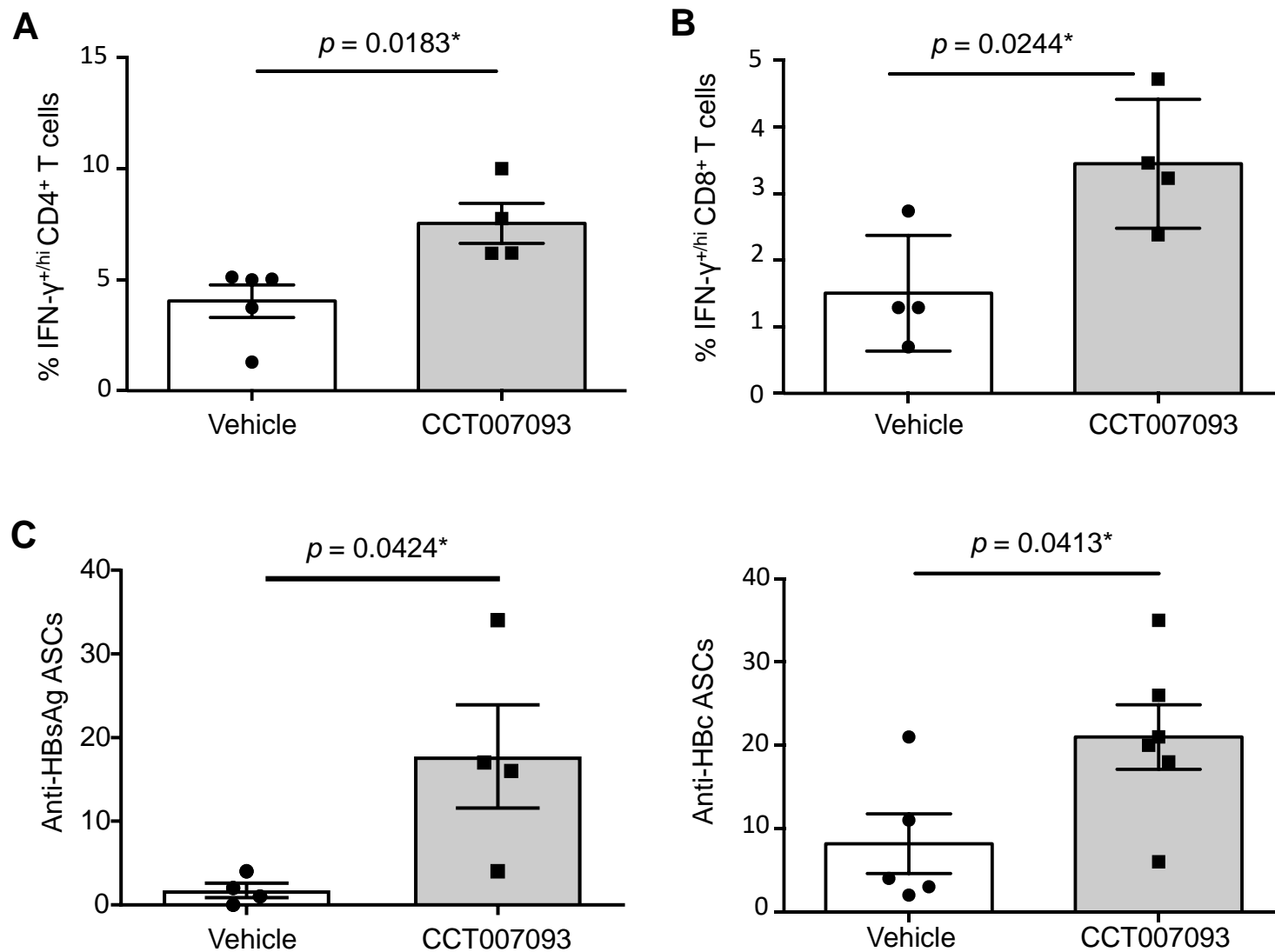


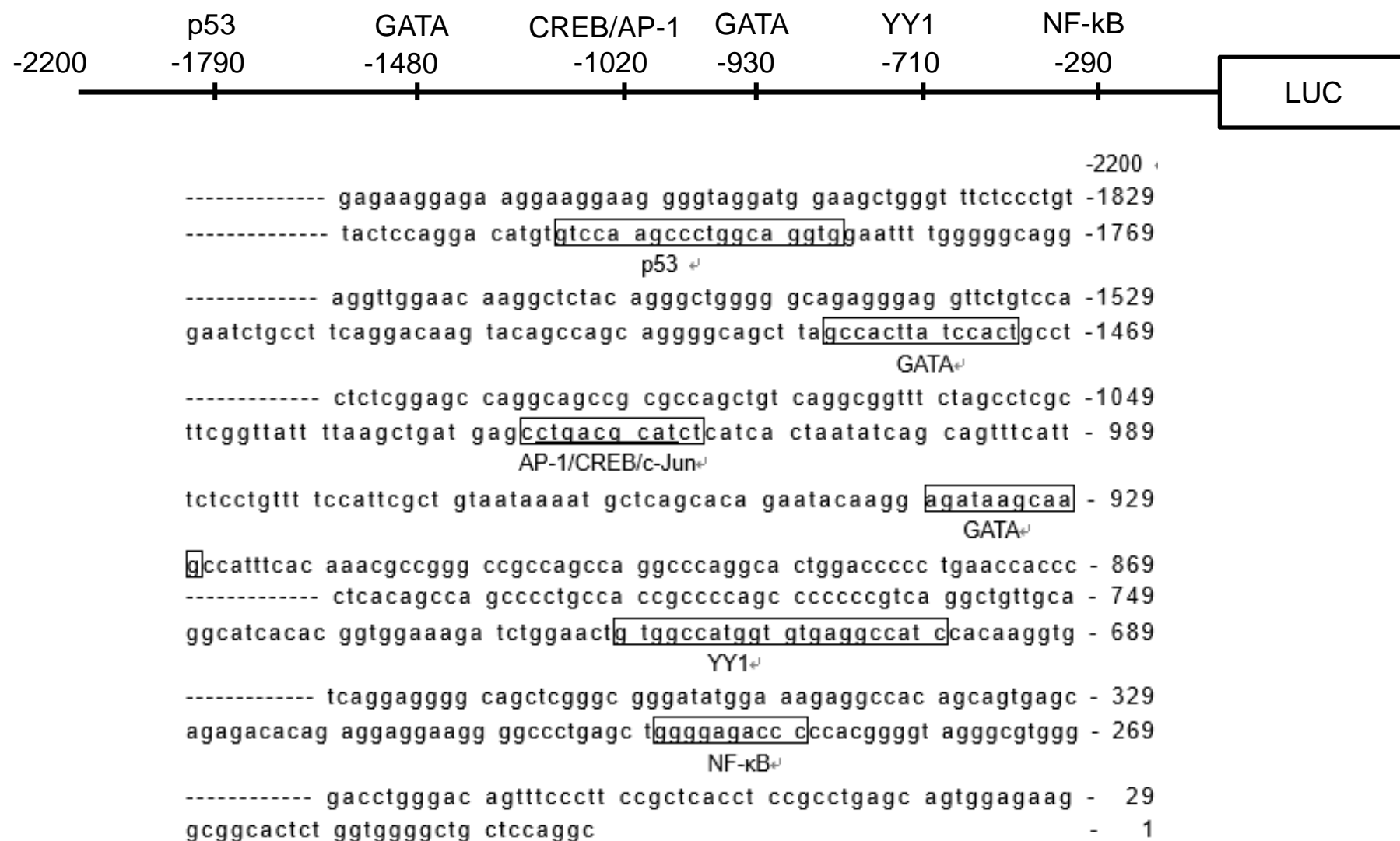


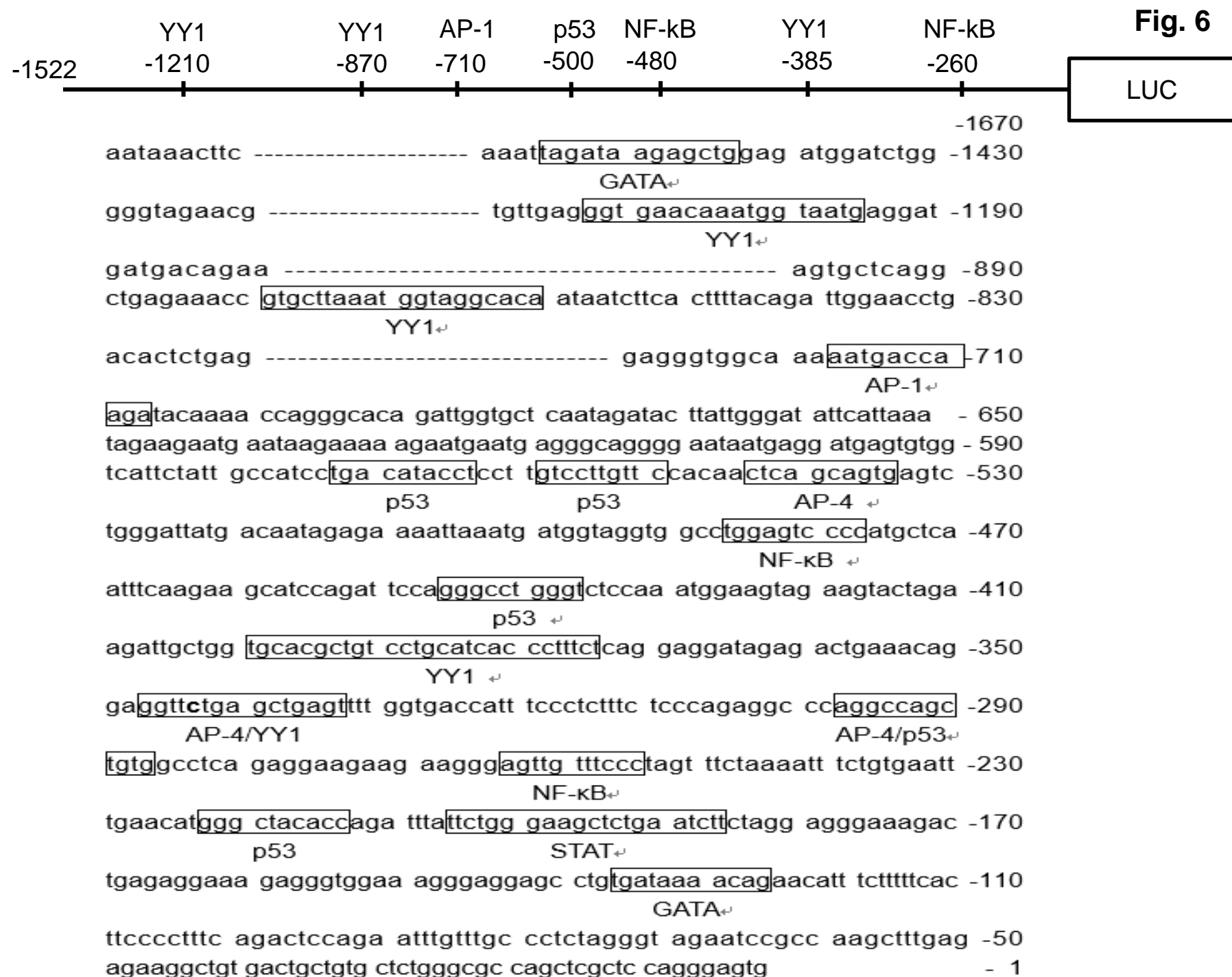
**Fig. 5**



A

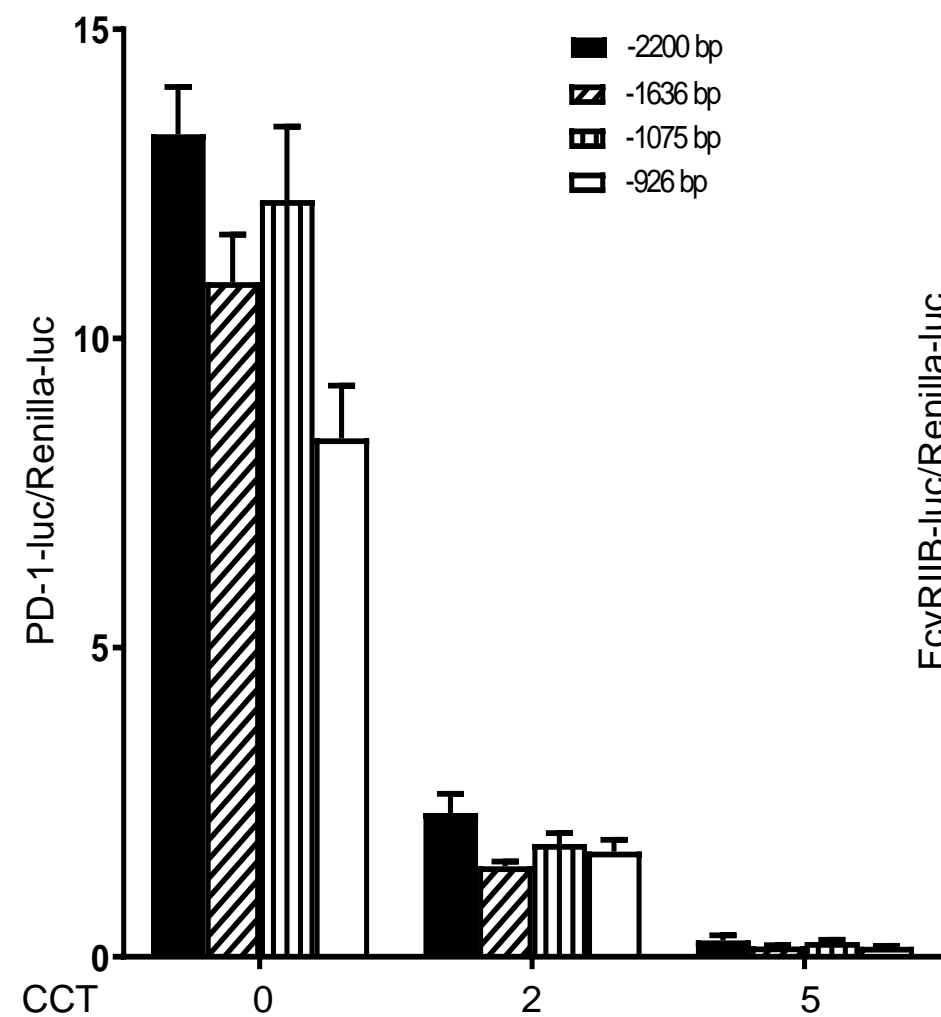
Fig. 6



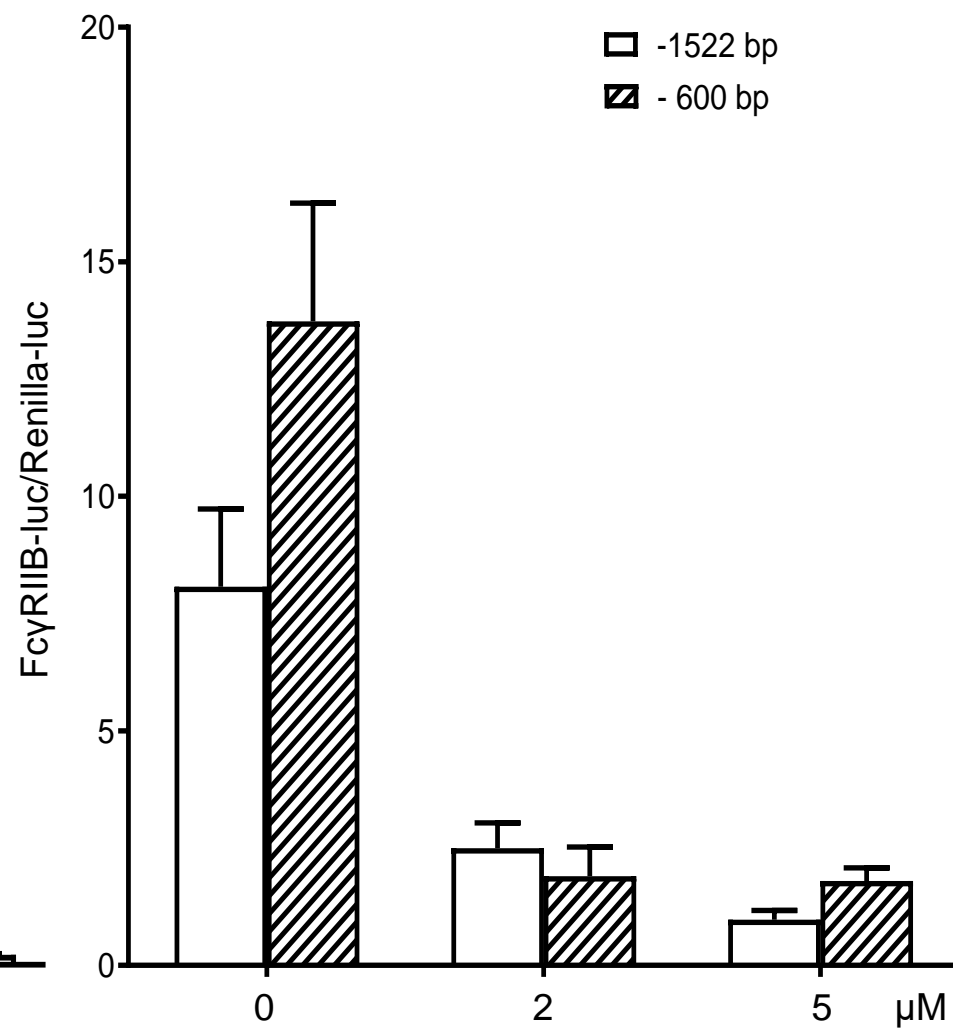
**B**

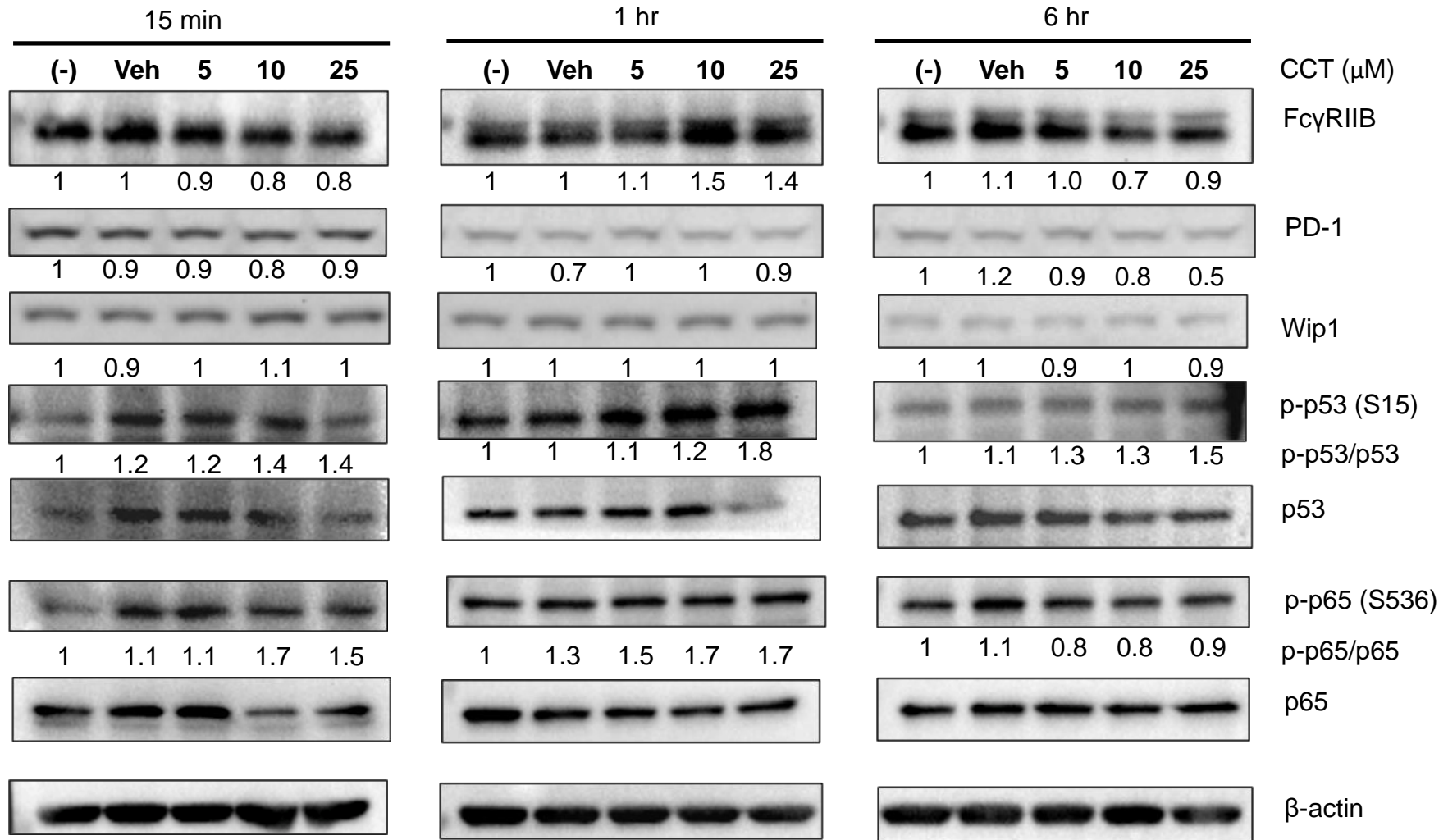
**Fig. 6**

**C**



**D**



**Fig. 7****A**

**Fig. 7****B**